

Geodesic Synthetic Control Methods for Random Objects and Functional Data

Daisuke Kurisu^{1,*}, Yidong Zhou^{2,*}, Taisuke Otsu³, and Hans-Georg Müller^{2,†}

¹Center for Spatial Information Science, The University of Tokyo, Japan

²Department of Statistics, University of California, Davis, USA

³Department of Economics, London School of Economics, UK

November 4, 2025

Abstract

We introduce a geodesic synthetic control method for causal inference that extends existing synthetic control methods to scenarios where outcomes are elements in a geodesic metric space rather than scalars. Examples of such outcomes include distributions, compositions, networks, trees and functional data, among other data types that can be viewed as elements of a geodesic metric space given a suitable metric. We extend this further to geodesic synthetic difference-in-differences that builds on the established synthetic difference-in-differences for Euclidean outcomes. This estimator generalizes both the geodesic synthetic control method and a previously proposed geodesic difference-in-differences method and exhibits a double robustness property. The proposed geodesic synthetic control method is illustrated through comprehensive simulation studies and applications to the employment composition changes following the 2011 Great East Japan Earthquake, and the impact of abortion liberalization policy on fertility patterns in East Germany. We illustrate the proposed geodesic synthetic difference-in-differences by studying the consequences of the Soviet Union’s collapse on age-at-death distributions for males and females.

Keywords: causal inference, Fréchet mean, geodesic metric space, program evaluation, synthetic difference-in-differences

*The first two authors contributed equally to this work and are listed alphabetically.

†Corresponding author: hgmuller@ucdavis.edu.

‡D.K. was supported in part by JSPS KAKENHI Grant Number 23K12456 and 25K00624. H.G.M. was partially supported by NSF grant DMS-2310450.

1 Introduction

Since the seminal work by [Abadie and Gardeazabal \(2003\)](#) and [Abadie et al. \(2010\)](#), synthetic control methods (SCMs) have been widely applied to evaluate causal effects of policy changes in settings with observational panel or longitudinal data. SCMs are designed for settings where some units are subject to a policy intervention while others are not, and their outcomes are observed before and after the intervention. In such settings, synthetic control units constructed utilizing some optimal weighting of control units are employed to control for unobserved trends in the outcome over time that are unrelated to the policy effect. The SCM has become popular in many areas and has been applied in various comparative case studies of policy interventions (see [Abadie \(2021\)](#) for a survey).

Following the above pioneering work, the SCM has been extended in various directions, including an SCM that incorporates a penalty term for pairwise matching discrepancies between the treated units and the control units ([Abadie and L'Hour, 2021](#)), a SCM for high-dimensional settings ([Robbins et al., 2017](#)), a connection with matrix completion methods ([Amjad et al., 2018](#)) and conformal inference and robust t -testing for SCMs ([Chernozhukov et al., 2021a,b](#)). A modification of the synthetic control estimator by incorporating a bias correction method for inexact matching was proposed by [Ben-Michael et al. \(2021\)](#) and for a staggered adoption setting by [Ben-Michael et al. \(2022\)](#), while [Arkhangelsky et al. \(2021\)](#) introduced a synthetic difference-in-differences (SDID) estimator that combines attractive features of the SCM and difference-in-differences (DID).

However, all of these developments primarily focused on Euclidean outcomes. In modern data analysis, one frequently encounters outcomes that may be inherently non-Euclidean, including distributional data ([Petersen and Müller, 2016](#); [Panaretos and Zemel, 2020](#); [Petersen et al., 2022](#)), compositional data ([Scealy and Welsh, 2011](#)), manifold-valued data ([Patrangenaru and Ellingson, 2015](#)), networks ([Severn et al., 2022](#); [Zhou and Müller, 2022](#)) and functional data ([Hsing and Eubank, 2015](#); [Wang et al., 2016](#)). Such data reside natu-

rally in metric spaces where one often imposes additional mild properties such as geodesicity, which is satisfied for nearly all outcomes of interest, including those mentioned above under appropriate metrics; common choices are the Wasserstein metric for distributional spaces, the Riemannian metric on spheres for compositional data and on more general manifolds for manifold-valued data, the Frobenius or power metric when representing networks through their graph Laplacians, and the L^2 metric for the case of functional data. The Frobenius and power metrics, among other metrics, are also commonly used for the space of symmetric positive-definite matrices, which may also appear as outcomes, for example when correlation structures between random vectors are outcomes of interest. Another type of potential interest is the tree spaces with the BHV metric (Billera et al., 2001). All of these are geodesic metric spaces, requiring specialized approaches for causal inference. The challenge here is that these spaces, with the exception of the Hilbert space where functional data are situated, are inherently nonlinear, i.e., one does not have available linear operations such as addition, subtraction and scalar multiplication on which most established methods rely. General approaches to address these challenges for data analysis in metric spaces are discussed in Dubey et al. (2024).

Addressing causal inference for outcomes in geodesic spaces is a recent but rapidly evolving area. Recent studies include estimators for average treatment effects (Lin et al., 2023), DID (Torous et al., 2024), SCMs (Gunsilius, 2023; Gunsilius et al., 2024), and regression discontinuity designs (Van Dijcke, 2025); all of these papers focus on the special case of distributional outcomes. Recent contributions addressing more general outcomes that can be viewed as elements of a general geodesic metric space include Kurisu et al. (2024) and Zhou et al. (2025), where in the latter a geodesic DID (GDID) approach was developed.

In this paper, we introduce a geodesic synthetic control method (GSC) designed for outcomes residing in geodesic metric spaces such as those mentioned above. The GSC frame-

work thus accommodates a broad array of outcomes residing in geodesic metric spaces. For the special case of distributional outcomes, GSC encompasses the distributional synthetic control framework of [Gunsilius \(2023\)](#) when using the Wasserstein metric. However, GSC also permits the use of alternative metrics in distribution space, as long as the metric space is geodesic. This includes the Fisher-Rao metric and many other distribution metrics of interest, thereby broadening the scope of analysis even for the special case of distributional outcomes.

We introduce a causal model suitable for the GSC and establish theoretical identification results for the causal effects of interest. Specific examples of causal models satisfying our assumptions in various common geodesic metric spaces illustrate the practical applicability of the proposed methodology. Additionally, we develop an augmented GSC, motivated by the augmented SCM introduced by [Ben-Michael et al. \(2021\)](#) for Euclidean outcomes. This extension is non-trivial due to the absence of linear algebraic structures in geodesic metric spaces; it necessitates the use of geodesic transport maps to construct our estimators.

We further propose a geodesic synthetic difference-in-differences (GSDID) estimator, extending the SDID methodology introduced by [Arkhangelsky et al. \(2021\)](#) for Euclidean outcomes. The GSDID estimator combines desirable properties of both the proposed GSC and the GDID developed by [Zhou et al. \(2025\)](#), which exhibits a double robustness property: even if the weighting schemes from either GSC or GDID individually fail to eliminate bias, their combination within the GSDID framework provides additional robustness. Moreover, the GSDID framework subsumes both the GSC and GDID as special cases.

We illustrate the efficacy of our proposed methods through comprehensive simulation studies and three real-world applications. These applications involve the employment composition changes following the 2011 Great East Japan Earthquake, the impact of abortion liberalization policy on fertility patterns in East Germany, and the health consequences of the Soviet Union’s collapse quantified through age-at-death distributions. These examples

underscore the flexibility, robustness, and practical applicability of the proposed geodesic synthetic control methodologies.

The paper is organized as follows. Section 2 provides a concise review of metric geometry and introduces several geodesic metric spaces relevant for simulations and empirical analyses. Section 3 presents the proposed GSC framework, including identification results and extensions to augmented GSC and GSDID. Implementation details and simulation studies for network and symmetric positive-definite matrix outcomes are described in Section 4. Section 5 illustrates the practical applicability of GSC through two empirical examples: analyzing changes in employment composition following the 2011 Great East Japan Earthquake, and assessing the impact of abortion liberalization on fertility patterns in East Germany. Finally, Section 6 concludes the paper. Proofs of the main theoretical results and additional materials are provided in the Supplementary Material.

2 Preliminaries on Metric Geometry

We review here some essential concepts from metric geometry that are needed to study outcomes in general metric spaces (\mathcal{M}, d) . A *curve* in \mathcal{M} is a continuous map $\gamma : [0, 1] \rightarrow \mathcal{M}$, whose length is defined as

$$\ell(\gamma) = \sup \sum_{i=0}^{I-1} d(\gamma(t_i), \gamma(t_{i+1})),$$

where the supremum is taken over all possible finite partitions $0 = t_0 \leq \dots \leq t_I = 1$. A curve γ is called a *geodesic* if it satisfies $d(\gamma(s), \gamma(t)) = |t-s|d(\gamma(0), \gamma(1))$ for all $s, t \in [0, 1]$. The metric space \mathcal{M} is called a *geodesic space* if, for any two points $\alpha, \beta \in \mathcal{M}$, there exists a geodesic connecting them, denoted $\gamma_{\alpha, \beta}$. If this geodesic is unique for every pair of points in \mathcal{M} , the space is referred to as a *unique geodesic space* (Bridson and Haefliger, 1999).

Examples of unique geodesic spaces that frequently arise in applications are as follows. We will revisit some of these example spaces in our simulation studies and empirical

applications.

Example 1 (Networks). *Consider the space of simple, undirected, weighted networks with m nodes. Each network can be uniquely represented by its graph Laplacian matrix. The space of graph Laplacians \mathcal{L} serves as a natural framework for characterizing network structures (Kolaczyk and Csárdi, 2014; Severn et al., 2022; Zhou and Müller, 2022). When endowed with the Frobenius metric, defined as $d_F(L_1, L_2) = \|L_1 - L_2\|_F$ for $L_1, L_2 \in \mathcal{L}$, the space \mathcal{L} becomes a unique geodesic space. In this setting, the geodesic between L_1 and L_2 is given by the linear interpolation $\gamma_{L_1, L_2}(t) = (1 - t)L_1 + tL_2$ for $t \in [0, 1]$.*

Example 2 (Compositional Data). *Compositional data, represented by vectors of non-negative proportions summing to one, reside in the simplex*

$$\Delta^{d-1} = \{\mathbf{y} \in \mathbb{R}^d : y_j \geq 0, \sum_{j=1}^d y_j = 1\}.$$

Adopting the square-root transformation provides a map from Δ^{d-1} to the positive orthant of the unit sphere \mathcal{S}_+^{d-1} (Scealy and Welsh, 2011), where the induced geodesic distance on \mathcal{S}_+^{d-1} is the arc-length distance

$$d_g(\mathbf{z}_1, \mathbf{z}_2) = \arccos(\mathbf{z}_1' \mathbf{z}_2),$$

with $\mathbf{z}_1, \mathbf{z}_2 \in \mathcal{S}_+^{d-1}$. Let $\theta = \arccos(\mathbf{z}_1' \mathbf{z}_2)$ be the angle between \mathbf{z}_1 and \mathbf{z}_2 and $\|\cdot\|$ be the standard Euclidean metric. The geodesic connecting \mathbf{z}_1 and \mathbf{z}_2 is then

$$\gamma_{\mathbf{z}_1, \mathbf{z}_2}(t) = \cos(t\theta)\mathbf{z}_1 + \sin(t\theta) \frac{\mathbf{z}_2 - (\mathbf{z}_1' \mathbf{z}_2)\mathbf{z}_1}{\|\mathbf{z}_2 - (\mathbf{z}_1' \mathbf{z}_2)\mathbf{z}_1\|}, \quad t \in [0, 1].$$

Example 3 (Symmetric Positive-Definite Matrices). *The space of $m \times m$ symmetric positive-definite (SPD) matrices, denoted by Sym_m^+ , plays a crucial role in various fields such as computer vision (Cherian and Sra, 2016), signal processing (Arnaudon et al., 2013) and neuroimaging (Dryden et al., 2009). Various metrics have been introduced to endow Sym_m^+ with a meaningful geometric structure, depending on the application. The Frobenius metric*

d_F induces unique geodesics that are simple linear interpolations, $\gamma_{A,B}(t) = (1-t)A + tB$ for $A, B \in \text{Sym}_m^+$ and $t \in [0, 1]$. The space Sym_m^+ also forms a unique geodesic space under various other metrics such as the Log-Euclidean metric (Arsigny et al., 2007), the power metric family (Dryden et al., 2009) or the Log-Cholesky metric (Lin, 2019). For instance, when adopting the log-Euclidean metric, the unique geodesic connecting $A, B \in \text{Sym}_m^+$ is given by

$$\gamma_{A,B}(t) = \exp\{(1-t)\log A + t\log B\}, \quad t \in [0, 1],$$

where $\exp(A)$ and $\log(A)$ are the matrix exponential and logarithmic maps for a real matrix A .

Example 4 (One-Dimensional Probability Distributions). Let \mathcal{W} denote the space of one-dimensional probability distributions on \mathbb{R} with finite second moments, equipped with the 2-Wasserstein distance

$$d_{\mathcal{W}}(\mu, \nu) = \left(\int_0^1 \{F_{\mu}^{-1}(s) - F_{\nu}^{-1}(s)\}^2 ds \right)^{1/2},$$

where F_{μ}^{-1} and F_{ν}^{-1} are the quantile functions of the probability measures μ and ν , respectively. The Wasserstein space \mathcal{W} is a complete, separable and unique geodesic space (Ambrosio et al., 2008), with geodesics given by McCann's interpolant (McCann, 1997)

$$\gamma_{\mu,\nu}(t) = \{\text{id} + t(F_{\nu}^{-1} \circ F_{\mu} - \text{id})\}_{\#}\mu, \quad t \in [0, 1],$$

where id denotes the identity map, F_{μ} is the cumulative distribution function of μ , and $\tau_{\#}\mu$ denotes the pushforward measure of μ by τ .

An alternative metric that is easy to compute for both univariate and multivariate distributions and is of some practical interest is the Fisher-Rao metric

$$d_{FR}(\mu, \nu) = \arccos \left(\int_{\mathbb{R}} \sqrt{f_{\mu}(x)f_{\nu}(x)} dx \right),$$

where f_{μ} and f_{ν} are the probability density functions of the measures μ and ν , respectively.

Example 5 (Functional Data). *In functional data analysis, one considers data consisting of functions that are considered to be the realizations of a square integrable stochastic process, usually assumed to be defined on a finite interval. Such data are common in the social, physical and life sciences (Ramsay and Silverman, 2005; Hsing and Eubank, 2015; Wang et al., 2016). Typically, functional data are assumed to be situated in the Hilbert space $L^2(\mathcal{T})$ of square integrable functions, where \mathcal{T} is a compact interval, most commonly a time domain. In contrast to the other metric spaces we consider in this paper, this space is a vector space and thus permits algebraic operations. It is equipped with the standard L^2 metric*

$$d_{L^2}(g_1, g_2) = \left(\int_{\mathcal{T}} \{g_1(t) - g_2(t)\}^2 dt \right)^{1/2}, \quad g_1, g_2 \in L^2(\mathcal{T}),$$

making $L^2(\mathcal{T})$ a unique geodesic space, with the unique geodesic between g_1 and g_2 given by

$$\gamma_{g_1, g_2}(t) = (1 - t)g_1 + tg_2, \quad t \in [0, 1].$$

3 Geodesic Synthetic Control Methods

3.1 Construction of the estimator

We begin with the conventional synthetic control method (SCM) for Euclidean outcomes. Suppose outcomes $Y_{j,t} \in \mathbb{R}^q$ are observed for $J + 1$ units over T time periods, indexed by $j = 1, \dots, J + 1$ and $t = 1, \dots, T$. Let $T_0 > 1$ denote the last pre-treatment period, and assume that only unit $j = 1$ receives the intervention for $t > T_0$. For unit j at time t , we denote potential outcomes under treatment and no treatment by $Y_{j,t}(I)$ and $Y_{j,t}(N)$, respectively. We observe $Y_{1,t} = Y_{1,t}(I)$ for $t > T_0$ and $Y_{j,t} = Y_{j,t}(N)$ otherwise. The causal effect of interest is

$$\tau_t = Y_{1,t}(I) - Y_{1,t}(N), \quad t = T_0 + 1, \dots, T.$$

In Euclidean settings, the synthetic control estimator constructs a convex combination of the control units that best reproduces the pre-treatment trajectory of the treated unit.

Let $\Delta^{J-1} = \{\mathbf{w} = (w_2, \dots, w_{J+1})' \in \mathbb{R}^J : w_j \geq 0, \sum_{j=2}^{J+1} w_j = 1\}$ denote the probability simplex, and $\bar{\mathbf{w}} = (\bar{w}_2, \dots, \bar{w}_{J+1})' \in \Delta^{J-1}$ be the optimal weight vector. The synthetic control outcome for the treated unit is defined as

$$Y_{1,t}^{(\text{SC})} = \sum_{j=2}^{J+1} \bar{w}_j Y_{j,t}, \quad t = T_0 + 1, \dots, T,$$

where the weights are chosen to minimize the mean squared pre-treatment discrepancy,

$$\bar{\mathbf{w}} \in \arg \min_{\mathbf{w} \in \Delta^{J-1}} \frac{1}{T_0} \sum_{t=1}^{T_0} \|Y_{1,t} - Y_{2:J+1,t}^{(\mathbf{w})}\|^2, \quad Y_{2:J+1,t}^{(\mathbf{w})} = \sum_{j=2}^{J+1} w_j Y_{j,t}.$$

The SCM estimator of the causal effect is then given by

$$\tau_t^{(\text{SC})} = Y_{1,t} - Y_{1,t}^{(\text{SC})}, \quad t = T_0 + 1, \dots, T.$$

The construction of SCM relies on two key components: the weighted mean of the control outcomes $Y_{2:J+1,t}^{(\mathbf{w})}$ and the difference $Y_{1,t} - Y_{1,t}^{(\text{SC})}$. Both are natural in Euclidean space but are not directly available for non-Euclidean outcomes, such as distributions or networks, where algebraic operations like addition, subtraction, or scalar multiplication are not defined. For metric spaces, the appropriate analogue of the weighted mean is the weighted Fréchet mean (Fréchet, 1948; Ginestet et al., 2012), defined for objects $Y_{2,t}, \dots, Y_{J+1,t} \in \mathcal{M}$ in a metric space (\mathcal{M}, d) as

$$Y_{2:J+1,t}^{(\mathbf{w})} = \arg \min_{\nu \in \mathcal{M}} \sum_{j=2}^{J+1} w_j d^2(\nu, Y_{j,t}),$$

which reduces to the weighted Euclidean average when $\mathcal{M} = \mathbb{R}^q$ and d is the Euclidean distance. For defining causal effects, differences are also not available outside Euclidean space. However, when the outcome space is geodesic, a suitable generalization exists: in Euclidean space, the difference $\beta - \alpha$ can be equivalently interpreted as movement along the straight line (geodesic) from α to β , which motivates defining causal effects via geodesics in geodesic metric spaces (Kurisu et al., 2024).

Accordingly, in a unique geodesic space (\mathcal{M}, d) we define the causal effect of the intervention as the geodesic connecting the untreated and treated potential outcomes,

$$\tau_t = \gamma_{Y_{1,t}(N), Y_{1,t}(I)}, \quad t = T_0 + 1, \dots, T. \quad (1)$$

The uniqueness of geodesics ensures that τ_t is well defined. This definition preserves the interpretation of τ_t as encoding both the distance and direction of change.

To estimate τ_t , we extend the weight construction from SCM using weighted Fréchet means. The synthetic control outcome for the treated unit is

$$Y_{1,t}^{(\text{GSC})} = \arg \min_{\nu \in \mathcal{M}} \sum_{j=2}^{J+1} \bar{w}_j d^2(\nu, Y_{j,t}),$$

with weights chosen as

$$\bar{\mathbf{w}} \in \arg \min_{\mathbf{w} \in \Delta^{J-1}} \frac{1}{T_0} \sum_{t=1}^{T_0} d^2 \left(Y_{1,t}, Y_{2:J+1,t}^{(\mathbf{w})} \right), \quad Y_{2:J+1,t}^{(\mathbf{w})} = \arg \min_{\nu \in \mathcal{M}} \sum_{j=2}^{J+1} w_j d^2(\nu, Y_{j,t}). \quad (2)$$

The geodesic synthetic control (GSC) estimator of the treatment effect is then

$$\tau_t^{(\text{GSC})} := \gamma_{Y_{1,t}^{(\text{GSC})}, Y_{1,t}} \quad t = T_0 + 1, \dots, T.$$

3.2 Causal model for the geodesic synthetic control method

To analyze the validity of the GSC estimator, we introduce a causal model describing the potential outcomes in the absence of treatment. In this framework, each unit j is associated with a latent characteristic $U_j \in \mathcal{M}$, where (\mathcal{M}, d) is the outcome space, and the untreated outcome at time t is generated as

$$Y_{j,t}(N) = g_t(U_j), \quad t = 1, \dots, T, \quad j = 1, \dots, J+1, \quad (3)$$

with $g_t : \mathcal{M} \rightarrow \mathcal{M}$ a measurable map that evolves outcomes over time.

In the special case where (\mathcal{M}, d) is the Euclidean space \mathbb{R}^q equipped with the standard Euclidean metric, geodesics are straight lines and the model simplifies to

$$g_t(U_j) = \mu_t + \alpha_t(U_j - \mu_t),$$

which corresponds to the linear factor model often used in the Euclidean SCM literature (Abadie et al., 2010). Thus the causal model (3) generalizes the familiar Euclidean setting of SCM to a broad class of metric spaces. When covariates are available, we consider an

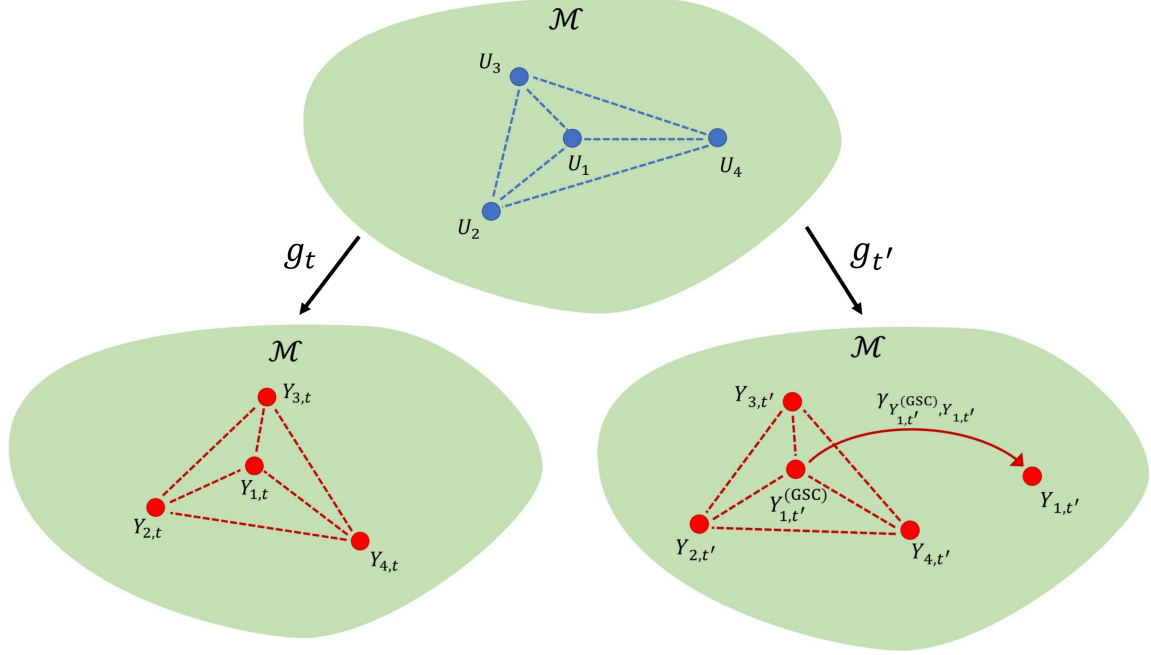


Figure 1: Illustration of the causal framework for the geodesic synthetic control method. Circles represent random objects in the metric space \mathcal{M} . For $t \leq T_0$ the treated outcome $Y_{1,t}$ is matched by a weighted Fréchet mean of controls. For $t' > T_0$ the estimator compares $Y_{1,t'}^{(\text{GSC})}$ with the observed $Y_{1,t'}$, the geodesic connecting them representing the estimated causal effect.

augmented version in Section 3.3 to address potential biases that arise when the pre-treatment fit is imperfect. Figure 1 provides an illustration of this framework.

We define the synthetic outcome for a weight vector $\mathbf{w} \in \Delta^{J-1}$ as

$$g_t^{(\mathbf{w})}(U_{2:J+1}) = \arg \min_{\nu \in \mathcal{M}} \sum_{j=2}^{J+1} w_j d^2(\nu, g_t(U_j)),$$

that is, the weighted Fréchet mean of the control outcomes at time t . The goal of synthetic control is to find weights \mathbf{w} such that this synthetic outcome reproduces the untreated outcome of the treated unit, $g_t(U_1)$.

For each time point t , let

$$\mathbb{W}_t^* = \{\mathbf{w} \in \Delta^{J-1} : d(g_t(U_1), g_t^{(\mathbf{w})}(U_{2:J+1})) = 0\}$$

denote the set of weight vectors that perfectly reconstruct U_1 at time t . We impose the following assumption, which is the direct analogue of the perfect pre-treatment fit assumption in Abadie et al. (2010).

Assumption 3.1.

- (i) For each $\mathbf{w} \in \Delta^{J-1}$ and $t = 1, \dots, T$, the weighted Fréchet mean $g_t^{(\mathbf{w})}(U_{2:J+1})$ exists uniquely.
- (ii) There exists a nonempty set of weights \mathbf{w} that achieve perfect fit in the pre-treatment period, i.e., $\bigcap_{t=1}^{T_0} \mathbb{W}_t^* \neq \emptyset$, and these same weights also reproduce U_1 in the post-treatment period, i.e., $\bigcap_{t=1}^{T_0} \mathbb{W}_t^* \subset \bigcap_{t=T_0+1}^T \mathbb{W}_t^*$.

Assumption 3.1(i) holds for the spaces discussed in Examples 1–5, and more generally for Hadamard spaces (Sturm, 2003), a broad class of non-positively curved spaces that possess unique geodesics. Assumption 3.1(ii) ensures that there is at least one set of weights \mathbf{w} that perfectly reconstructs the treated unit in the pre-treatment period, and that this same set of weights also remains valid in the post-treatment period. This is the natural analogue of the perfect pretreatment fit condition in Abadie et al. (2010), now formulated for general geodesic spaces.

Assumption 3.1(ii) can be verified in a wide class of models. One example is

$$g_t(U_j) = \gamma_{\mu_t, U_j}(\alpha_t), \quad \mu_t \in \mathcal{M}, \quad \alpha_t \in (0, 1),$$

where outcomes are obtained by moving along the geodesic from a reference point μ_t toward U_j by a proportion α_t . This model can be shown to hold in networks (Example 1), the Wasserstein space (Example 4), functional data (Example 5), and in the space of symmetric positive-definite matrices (Example 3) equipped with the Frobenius metric, the power metric family, the Log-Euclidean metric, or the Log-Cholesky metric. For compositional data on the sphere \mathcal{S}_+^{d-1} (Example 2), Assumption 3.1 can be verified under models of the form

$$g_t(U_j) = \text{Exp}_{\mu_t}(A_t \text{Log}_{\mu_t}(U_j)),$$

where A_t is a $(d-1) \times (d-1)$ positive-definite matrix, and Exp_μ and Log_μ denote the Riemannian exponential and logarithmic maps at $\mu \in \mathcal{M}$. Further details for these cases

are provided in Section S.4 of the Supplementary Material.

The following result establishes model identification of the GSC.

Theorem 3.1. *Suppose that Assumption 3.1 holds for model (3). Then $Y_{1,t}^{(\text{GSC})} = Y_{1,t}(N)$ for each $t = T_0 + 1, \dots, T$.*

It is also possible to extend the model (3) to the case where the latent characteristics U_j vary over time, i.e., $Y_{j,t}(N) = g_t(U_{j,t})$ with $U_{j,t} \in \mathcal{M}$. In this setting, a result similar to Theorem 3.1 holds provided that the sets $\mathbf{W}_t^* = \{\mathbf{w} \in \Delta^{J-1} : d(g_t(U_{1,t}), g_t^{(\mathbf{w})}(U_{2:J+1,t})) = 0\}$ satisfy a modified version of Assumption 3.1(ii).

Remark 3.1 (Geodesic synthetic control with negative weights). *Instead of restricting to weights in the simplex Δ^{J-1} , one may also allow weights in the affine simplex*

$$\Sigma^{J-1} = \{\mathbf{w} = (w_2, \dots, w_{J+1})' \in \mathbb{R}^J : \sum_{j=2}^{J+1} w_j = 1\},$$

which permits negative components. If such weights satisfy a condition analogous to Assumption 3.1(ii), identification results remain unchanged. However, negative weights can lead to overfitting of pre-treatment outcomes, and regularization or penalization, as in Arkhangelsky et al. (2021), may be needed to improve out-of-sample performance.

Remark 3.2 (Geodesic synthetic control method with covariates). *Suppose covariates $\{X_{j,t} \in (\mathcal{M}_X, d_X) : j = 1, \dots, J+1, t = 1, \dots, T\}$ are available, where the covariate space (\mathcal{M}_X, d_X) may differ from the outcome space (\mathcal{M}, d) and often corresponds to \mathbb{R}^q with the Euclidean metric. In this case, the construction of the GSC weights can be modified to account for covariates. Specifically, we define*

$$\tau_t^{(\text{COV})} := \gamma_{Y_{1,t}^{(\text{COV})}, Y_{1,t}}, \quad t = T_0 + 1, \dots, T,$$

where the synthetic control outcome is given by

$$Y_{1,t}^{(\text{COV})} = \arg \min_{\nu \in \mathcal{M}} \sum_{j=2}^{J+1} \bar{w}_j(X) d^2(\nu, Y_{j,t}),$$

and the covariate-dependent weights are chosen as

$$\overline{\mathbf{w}}(X) \in \arg \min_{\mathbf{w} \in \Delta^{J-1}} \frac{1}{T_0} \sum_{t=1}^{T_0} d_X^2(X_{1,t}, X_{2:J+1,t}^{(\mathbf{w})}), \quad X_{2:J+1,t}^{(\mathbf{w})} = \arg \min_{\nu \in \mathcal{M}} \sum_{j=2}^{J+1} w_j d_X^2(\nu, X_{j,t}).$$

If multiple covariates are available, say $X_{j,t} = (X_{j,t}^{(1)}, \dots, X_{j,t}^{(k)})$, one can work in the product space $\mathcal{M}_X = \mathcal{M}_1 \times \dots \times \mathcal{M}_k$ with combined metric $d_X^2 = d_1^2 + \dots + d_k^2$. This construction extends the covariate-adjusted SCM approach of [Abadie et al. \(2010\)](#) from Euclidean outcomes to general metric spaces.

Remark 3.3 (Placebo permutation test). In order to formally test for the presence of a causal effect, one may employ a placebo permutation test ([Abadie, 2021](#)). In addition to the synthetic control outcome $Y_{1,t}^{(\text{GSC})}$, we compute $Y_{j,t}^{(\text{GSC})}$ for $j = 2, \dots, J+1$ by applying the same algorithm as used to obtain $Y_{1,t}^{(\text{GSC})}$, pretending the treatment unit is j . If there is an actual treatment effect only in unit $j = 1$, then the distance $d(Y_{1,t}, Y_{1,t}^{(\text{GSC})})$ for the actual treatment unit should be among the most extreme in $\{d(Y_{j,t}, Y_{j,t}^{(\text{GSC})}) : j = 1, \dots, J+1\}$. In this framework, the p -value for testing the null hypothesis of no causal effect by the intervention to unit $j = 1$ is

$$\frac{\text{rank of } d(Y_{1,t}, Y_{1,t}^{(\text{GSC})}) \text{ in } \{d(Y_{j,t}, Y_{j,t}^{(\text{GSC})}) : j = 1, \dots, J+1\}}{J+1}, \quad t = T_0 + 1, \dots, T.$$

3.3 Augmented geodesic synthetic control method

In some applications, the untreated outcome $Y_{1,t}(N)$ may not lie in the convex hull of the controls $\{Y_{2,t}, \dots, Y_{J+1,t}\}$, so that $Y_{1,t}(N) \neq Y_{2:J+1,t}^{(\mathbf{w})}$ for any $\mathbf{w} \in \Delta^{J-1}$. In this case, the GSC estimator can be biased for the true causal effect τ_t . To address this issue, we propose an augmented version of GSC, which parallels the regression-adjusted synthetic control of [Ben-Michael et al. \(2021\)](#) and reduces bias when covariates are available.

The development of augmented GSC builds upon the notion of a geodesic transport map ([Zhu and Müller, 2023](#)), which ensures that the geodesic joining points α and β can be naturally extended from any other point $\omega \in \mathcal{M}$. Formally, a geodesic transport map

$\Gamma_{\alpha,\beta} : \mathcal{M} \rightarrow \mathcal{M}$ satisfies $\Gamma_{\alpha,\beta}(\alpha) = \beta$ and provides a natural way to “shift” points in \mathcal{M} according to the displacement from α to β . In Euclidean space, this reduces to the familiar translation $\Gamma_{\alpha,\beta}(\omega) = \omega + (\beta - \alpha)$, while in more general spaces it corresponds to parallel transport or its analogues. The existence of such maps is ensured in a wide range of spaces of practical interest.

Building on this idea, the augmented GSC corrects the bias of the standard GSC by transporting its synthetic prediction along a geodesic determined by pre-treatment regression adjustment. For Euclidean outcomes, the resulting estimator reduces exactly to the augmented synthetic control estimator of [Ben-Michael et al. \(2021\)](#), while for general geodesic spaces it provides a natural extension that preserves the same logic of bias correction.

For full details, including the formal definition of geodesic transport maps, concrete examples, and the detailed derivation of the augmented GSC estimator, we refer to Section S.1 of the Supplementary Material.

3.4 Extension to geodesic synthetic difference-in-differences

In addition to GSC and its augmented version, we also develop a geodesic extension of the synthetic difference-in-differences framework of [Arkhangelsky et al. \(2021\)](#). The proposed geodesic synthetic difference-in-differences (GSDID) estimator combines unit weights with time weights, thereby merging the advantages of GSC with the geodesic difference-in-differences of [Zhou et al. \(2025\)](#). This construction addresses bias that cannot be removed by unit reweighting alone, making use of both cross-sectional and temporal information. A notable property of GSDID is double robustness: even if either the unit-weighting scheme or the time-weighting scheme fails individually, their combination can still provide a valid adjustment.

The full methodology, including theoretical identification results and estimation details,

is provided in Section S.2 of the Supplementary Material. To illustrate the proposed approach, we also include a real-data application that investigates the causal effect of the collapse of the Soviet Union on Russian mortality using age-at-death distributions and the Wasserstein metric. This example demonstrates how GSDID can capture complex causal effects for distributional outcomes in geodesic metric spaces.

4 Implementation and Simulations

4.1 Implementation details

Algorithm 1 outlines the implementation steps for the proposed geodesic synthetic control method. The optimization problem in Step 1 of Algorithm 1 requires customized approaches that depend on the specific metric and geometry of the underlying metric space. For networks (Example 1), symmetric positive-definite matrices (Example 3), distributions (Example 4), and functions (Example 5), the optimization reduces to a straightforward convex quadratic optimization problem that can be easily implemented (Stellato et al., 2020).

For the case of compositional data (Example 2), the optimization becomes more challenging, as it involves minimizing a bilevel objective where the weighted Fréchet mean $Y_{2:J+1,t}^{(w)}$ is itself an argmin problem. Due to the complexity of analytical differentiation when nonlinear Fréchet means are involved, we adopt a derivative-free constrained optimization strategy. Specifically, we use the Constrained Optimization BY Linear Approximations (COBYLA) algorithm (Powell, 1994), as implemented in the R package `nloptr` (Johnson, 2008). The weighted Fréchet mean involved in the objective function is obtained using the R package `manifold` (Dai et al., 2021). Further computational details, including explicit formulations of the optimization problems and solver strategies across different geodesic metric spaces, are provided in Section S.3 of the Supplementary Material.

Algorithm 1: Geodesic Synthetic Control Method

Input: data $\{Y_{j,t} : j = 1, \dots, J+1, t = 1, \dots, T\}$.

Output: geodesic synthetic control estimator $\tau_t^{(\text{GSC})}$ for $t = T_0 + 1, \dots, T$.

1 $\bar{\mathbf{w}} = (\bar{w}_2, \dots, \bar{w}_{J+1}) \leftarrow$ the estimated synthetic control weights:

$$\bar{\mathbf{w}} \in \arg \min_{\mathbf{w} \in \Delta^{J-1}} \frac{1}{T_0} \sum_{t=1}^{T_0} d^2(Y_{1,t}, Y_{2:J+1,t}^{(\mathbf{w})})$$

where $Y_{2:J+1,t}^{(\mathbf{w})} = \arg \min_{\nu \in \mathcal{M}} \sum_{j=2}^{J+1} w_j d^2(\nu, Y_{j,t})$ for $t = 1, \dots, T_0$;

2 $Y_{1,t}^{(\text{GSC})} = \arg \min_{\nu \in \mathcal{M}} \sum_{j=2}^{J+1} \bar{w}_j d^2(\nu, Y_{j,t}) \leftarrow$ the synthetic control unit;

3 $\tau_t^{(\text{GSC})} = \gamma_{Y_{1,t}^{(\text{GSC})}, Y_{1,t}} \leftarrow$ the geodesic synthetic control estimator.

4.2 Simulations for networks and symmetric positive-definite matrices

We conduct simulations to assess the performance of the proposed geodesic synthetic control method using networks and SPD matrices. Potential outcomes without intervention are generated via the geodesic model $Y_{j,t}(N) = \gamma_{\mu_t, U_j}(\alpha_t)$, where $\mu_t, U_j \in \mathcal{M}$ represent the deterministic time trend and the unit-specific latent characteristic, respectively. We consider a total of $T = 20$ time periods, where the treatment occurs at $T_0 = 19$, and $J = 20$ control units. The primary goal of these simulations is to evaluate how accurately the synthetic control estimator $Y_{1,T}^{(\text{GSC})}$ replicates the true counterfactual $Y_{1,T}(N)$ for the treated unit at time T .

For the network outcomes, we use graph Laplacians residing in the space \mathcal{L} equipped with the Frobenius metric (see Example 1). Networks are simulated via a weighted stochastic block model with 10 nodes divided into two equal-sized communities. Edges within and between communities are generated using Bernoulli distributions with probabilities specified by the edge probability matrix $\begin{pmatrix} 0.75 & 0.1 \\ 0.1 & 0.75 \end{pmatrix}$. The weights of existing edges are generated as $\sin(0.1\pi t) + e^{-0.1t}((0.1j - 0.5)^2 - \sin(0.1\pi t))$. The graph Laplacian associated with each network is then considered to be the outcome.

For outcomes in the space of SPD matrices Sym_m^+ equipped with the Log-Euclidean metric (see Example 3), we generate the underlying SPD matrices μ and U from a Wishart distribution with 12 degrees of freedom and a scale matrix of $0.1\mathbf{I}_{10}$, where \mathbf{I}_{10} denotes the 10×10 identity matrix. The deterministic time trend and the unit-specific latent characteristic are constructed as $\mu_t = 0.1t\mu$ and $U_j = e^{(0.1j-0.5)^2}U$, respectively. The parameter α_t governing the geodesic interpolation is set to $\alpha_t = \log(0.1(t+1))$.

The counterfactual outcome for the treated unit had it not received the treatment $Y_{1,T}(N)$ and the synthetic control unit $Y_{1,T}^{(\text{GSC})}$ for networks and SPD matrices are illustrated in Figure 2. The synthetic control outcome precisely matches the true counterfactual outcome in both scenarios, highlighting the effectiveness of the GSC approach for outcomes located in complex geodesic metric spaces. These simulation results further validate the model identification established in Theorem 3.1.

5 Real Data Examples

5.1 Impact of the 2011 Great East Japan Earthquake on Employment- Population Ratio by Industry

We analyze the impact of the 2011 Great East Japan Earthquake on the employment-population ratio by employment category, using data from the Research Institute of Economy, Trade and Industry (RIETI) database (<https://www.rieti.go.jp/jp/database/R-JIP2021/index.html>). These data provide annual employment figures by industry for each prefecture in Japan from 1994 to 2018. Employment is categorized into three broad groups: primary (agriculture, forestry, and fisheries), secondary (manufacturing, electricity, gas, water supply, waste management and construction) and tertiary (services, including wholesale/retail, finance, and healthcare). For each prefecture and each year, the employment shares (proportions) across these three categories are represented as a three-

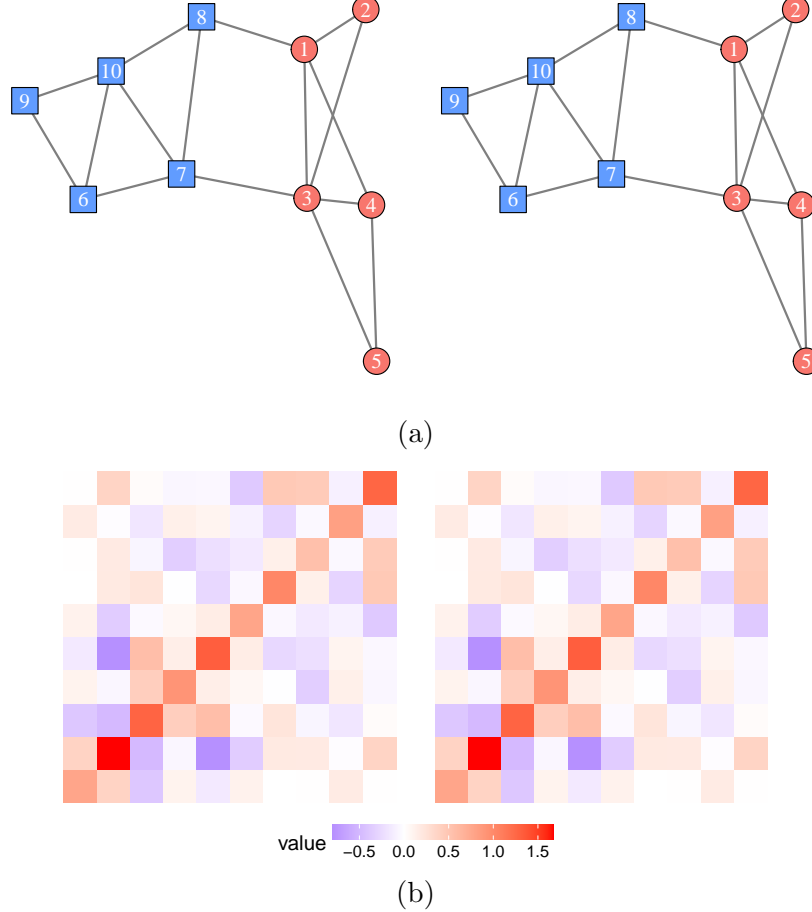


Figure 2: Simulated counterfactual outcome for the treated unit had it not received the treatment $Y_{1,T}(N)$ (left) and the corresponding synthetic control outcome $Y_{1,T}^{(GSC)}$ (right) using the proposed method for (A) networks and (B) SPD matrices. For networks, nodes from the two communities are represented by red circles and blue squares, respectively. For SPD matrices, outcomes are visualized as heatmaps.

dimensional compositional vector. The component-wise square root transformation (see Example 2) maps these compositional outcomes onto the positive quadrant of the sphere $S^2_+ \subset \mathbb{R}^3$, which we endow with the geodesic metric. Unlike standard synthetic control approaches that typically analyze each compositional component separately, the proposed approach considers the entire compositional vector jointly. This holistic perspective reflects the intrinsic geometry of compositional data, thereby capturing interdependencies of employment across the three categories.

The Great East Japan Earthquake occurred on March 11, 2011, causing widespread

devastation, particularly in Miyagi Prefecture, which suffered the highest number of fatalities. The earthquake significantly disrupted economic activity, leading to structural shifts in employment. To assess the impact of the earthquake on employment composition, we define Miyagi Prefecture as the treated unit, while control units are selected from prefectures located on Japan’s main island with a population between 1 million and 4 million in 2010, excluding the heavily affected areas of Fukushima, Iwate, and Miyagi. This results in a control group consisting of 19 prefectures: Akita, Gifu, Gunma, Hiroshima, Ibaraki, Ishikawa, Kyoto, Mie, Nagano, Nara, Niigata, Okayama, Shiga, Shizuoka, Tochigi, Toyama, Wakayama, Yamagata and Yamaguchi. The analysis considers the period 2008–2010 as pre-treatment and 2011–2013 as post-treatment to capture the immediate effects of the earthquake on employment composition.

We apply the proposed GSC to estimate the causal effect of the earthquake. The method constructs a synthetic counterpart for Miyagi Prefecture as a weighted combination of control prefectures, ensuring that the pre-treatment employment composition in the synthetic unit closely matches that of Miyagi. Figure 3 visualizes the employment compositions for Miyagi and control prefectures using a ternary plot. The results indicate that the proportion of secondary category employment increased following the earthquake, while the proportion of tertiary category employment declined.

This shift is likely driven by large-scale reconstruction efforts. The destruction of infrastructure and housing spurred demand for construction-related jobs, leading to growth in secondary category employment. Meanwhile, many service-based businesses, particularly in retail and hospitality, faced prolonged disruptions due to physical damage, population displacement and reduced consumer demand. Additionally, some workers may have transitioned from the service sector to reconstruction-related employment, further contributing to the observed shift. These findings suggest that the earthquake temporarily reshaped the labor market, emphasizing reconstruction at the expense of service-oriented employment.

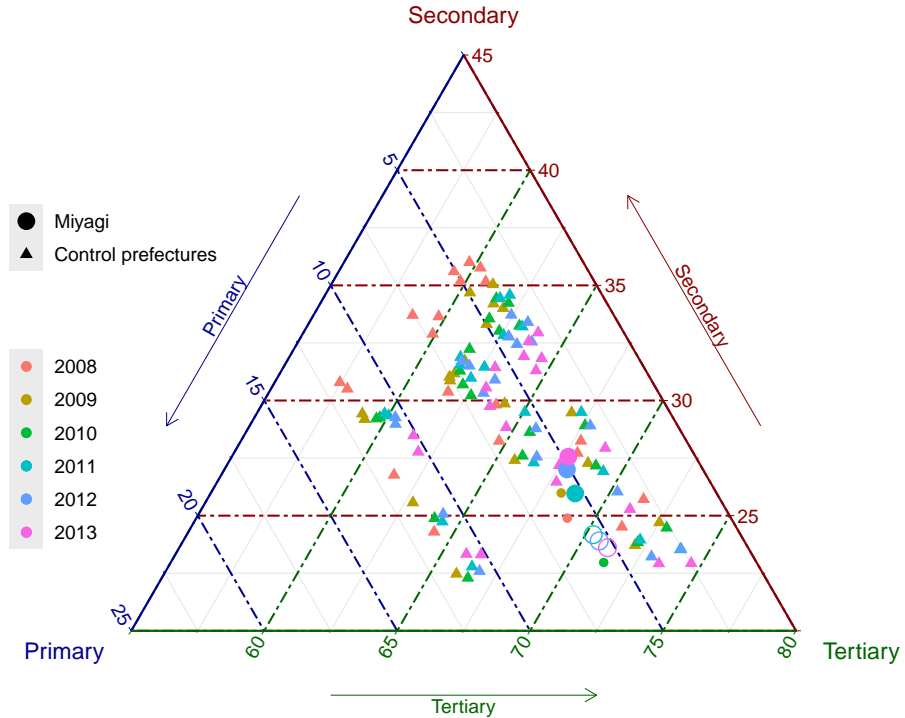


Figure 3: Ternary plot depicting employment compositions, where employment composition in the treated unit, Miyagi, is represented by circles, while employment compositions in the control prefectures are shown as triangles. Different years are distinguished by color. The synthetic controls for the post-treatment periods 2011, 2012 and 2013 are shown as hollow circles and are distinguished from the observed employment compositions for these years by a similar proportion of primary category employment, an increased proportion of secondary category employment and a reduced proportion of tertiary category employment.

The observed employment compositions for Miyagi in the primary, secondary and tertiary category for 2011 are $(0.053, 0.260, 0.687)'$, for 2012 they are $(0.051, 0.270, 0.679)'$ and for 2013 they are $(0.048, 0.276, 0.676)'$, while the geodesic synthetic compositions obtained for the same years are $(0.055, 0.242, 0.703)'$, $(0.055, 0.239, 0.706)'$, and $(0.053, 0.236, 0.711)'$. The effect of the earthquake on employment composition appears to have been less pronounced in 2011, likely due to the timing of the disaster on March 11, 2011, with immediate disruptions offset by short-term stabilization efforts. The impact became more pronounced in 2012 and 2013, reflecting longer-term shifts in employment patterns. To assess the statistical significance of this effect, we applied the placebo permutation test described in

Remark 3.3. The resulting p -values for the null hypothesis of no causal effect were 0.1 for 2011, 0.05 for 2012, and 0 for 2013. These results indicate that the immediate impact in 2011 was not strongly significant, but the earthquake's effect on Miyagi's employment composition became statistically significant starting from 2012.

5.2 Impact of the 1972 Abortion Legislation on Fertility Patterns in East Germany

The study of fertility rates has attracted substantial attention, with an increasing emphasis on analyzing age-specific fertility rates (ASFR) rather than relying solely on summary measures such as total fertility rate (Chen et al., 2017). Represented as fertility curves across reproductive ages, ASFR provides richer insights into fertility behaviors, allowing researchers to detect age-specific causal effects that aggregate statistics alone cannot capture. For example, a policy intervention might disproportionately influence fertility behaviors among younger women, information that is lost when relying solely on aggregate metrics.

In March 1972, East Germany introduced legislation permitting women to terminate pregnancies within the first twelve weeks, significantly liberalizing abortion access. Although the primary intention was reproductive autonomy, an unintended consequence was a substantial drop in fertility, with the total fertility rate decreasing notably from 2.1 children per woman in 1971 to 1.5 by 1975 (Büttner and Lutz, 1990). To gain deeper insights into how this policy affected fertility behavior across different reproductive ages, we applied the proposed GSC to ASFR curves. When viewed as functions over reproductive ages, these are functional data in the space L^2 (see Example 5).

The data for this analysis were obtained from the [Human Fertility Database](#), which provides ASFR annually for ages 12 to 55 for each calendar year across different countries. We select East Germany as the treated unit, given its distinct policy change, and utilize

a control group composed of 26 countries that did not experience comparable abortion liberalization during this period (Austria, Belgium, Bulgaria, Belarus, Canada, Switzerland, Czechia, Denmark, Spain, Estonia, Finland, France, Hungary, Iceland, Ireland, Italy, Japan, Lithuania, Netherlands, Portugal, Russia, Slovakia, Sweden, Ukraine, United Kingdom (England and Wales), and United States). We define 1965–1971 as pre-treatment periods and 1972–1975 as post-treatment periods, so that it is possible to capture both immediate and medium-term policy impacts. Figure 4 visualizes the ASFR curves for East Germany and the control countries from 1966 to 1975 using heat maps. A clear reduction in fertility rates is evident for East Germany during the post-treatment period (1972–1975) but other countries also experience reductions in fertility between 1965 and 1975.

Figure 5 compares the observed ASFR of East Germany with the synthetic control unit constructed from the control countries. Visual inspection suggests that the synthetic control closely tracks East Germany’s pre-treatment fertility patterns. After the policy implementation in 1972, East Germany exhibits a notable downward shift in fertility rates across prime childbearing ages (approximately ages 20–30), as reflected in the divergence from the synthetic control unit.

To assess the statistical significance of these observed differences, we applied the placebo permutation test by repeatedly applying the synthetic control procedure to each control country as if it had been treated. The resulting p -values for the null hypothesis of no causal effect in each post-treatment year (1972–1975) are 0.15, 0.11, 0.00, and 0.04, respectively. These results indicate that the immediate impact in 1972 and 1973 is not strongly significant; however, the fertility reduction becomes statistically significant in 1974. This confirms that the 1972 abortion policy had a substantial causal effect on fertility behavior in East Germany.

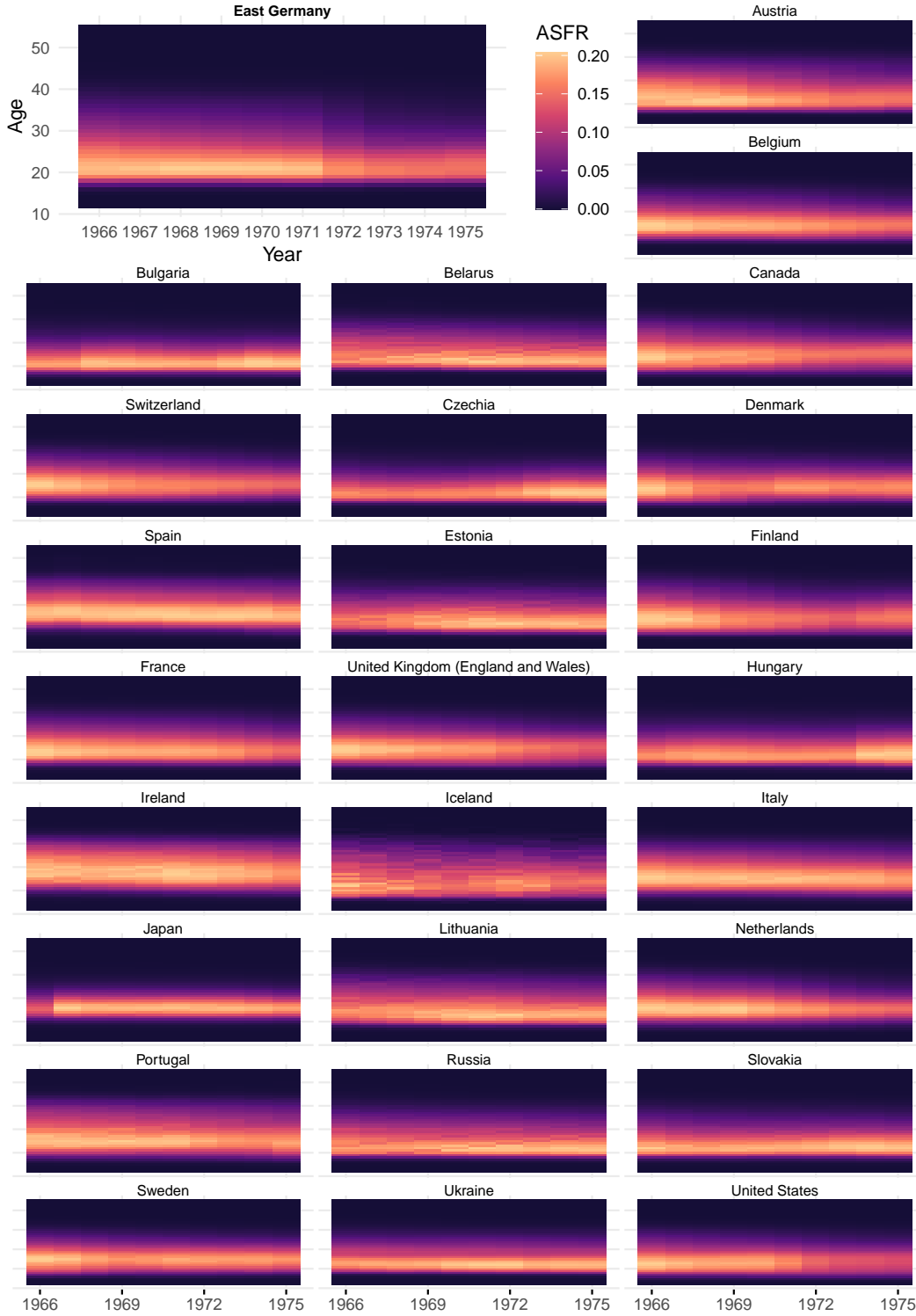


Figure 4: Age-specific fertility rates (ASFR) for East Germany and the control countries from 1966 to 1977 shown as heat maps. For each of the countries, each column represents the ASFR across ages 12 to 55 for a given calendar year that is indicated at the bottom of the figure.

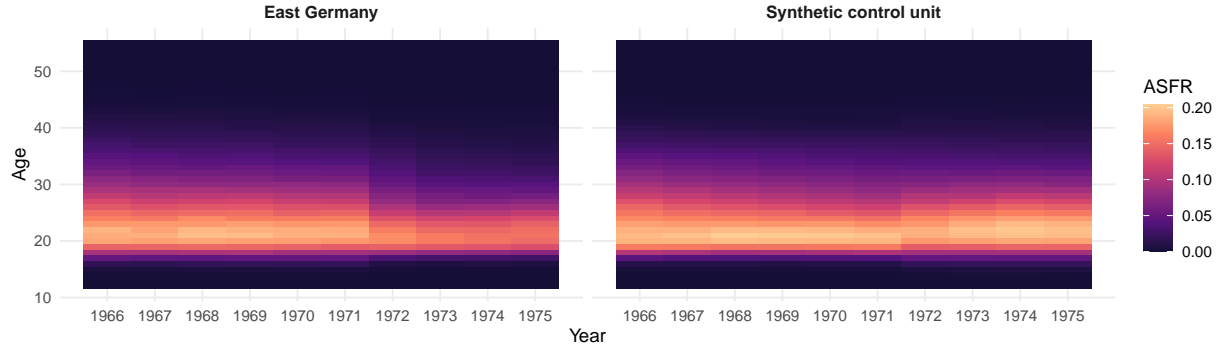


Figure 5: Heat maps of age-specific fertility rates (ASFR) for East Germany (left) and the synthetic control unit (right) from 1966 to 1975. Each column represents the ASFR across ages 12 to 55 (vertical axis) for each calendar year (horizontal axis).

6 Discussion and Concluding Remarks

A general causal model for outcomes that can be viewed as random objects, i.e., elements located in a suitable geodesic metric space, is the proposed geodesic synthetic difference-in-differences model (GSDID). It features the geodesic synthetic control method (GSC) and the geodesic difference-in-differences model (GDID) as special cases. As we demonstrate, the proposed geodesic models can be utilized to investigate various causal effects for economically relevant outcomes that are not Euclidean such as outcomes that correspond to compositions or networks. Even for infinite-dimensional Euclidean or near-Euclidean outcomes such as functional data and distributional data the proposed GSDID model is novel and is expected to be a useful addition to the toolbox for causal analysis.

An important modeling choice in this paper is to define the treatment effect as the geodesic between the potential outcomes $Y_{1,t}(N)$ and $Y_{1,t}(I)$. This extends the familiar Euclidean estimand $Y_{1,t}(I) - Y_{1,t}(N)$ to general spaces while preserving both magnitude and directional information. Most spaces of practical interest, including those considered in this paper, are unique geodesic spaces, so the effect is well defined. In cases where geodesics are not globally unique, one is typically interested in subsets where uniqueness holds—for example, the positive orthant of the hypersphere for compositional data. Alternative causal targets can also be considered, such as reporting the pair $(Y_{1,t}(I), Y_{1,t}^{(GSC)})$ or the

scalar distance $d(Y_{1,t}(I), Y_{1,t}(N))$, in which case only a general metric structure is required. Uniqueness becomes essential, however, for the augmented GSC and GSDID extensions, where geodesic transport maps play a central role.

Practical implementation of the proposed methods also calls for suitable diagnostic tools. Standard checks from the Euclidean SCM can be adapted to the geodesic setting. These include examining pre-treatment fit by plotting $d(Y_{1,t}, Y_{1,t}^{(\text{GSC})})$ over $t \leq T_0$, considering transformations (Ferman and Pinto, 2021) such as demeaning from the Fréchet mean when fit is poor, and using backdating to detect anticipation effects. Robustness can be further assessed through leave-one-out analyses of the control units. Together, these diagnostics help evaluate the credibility of counterfactual predictions in applications.

There are several directions for future research. Given a specific type of non-Euclidean outcome one often has a choice of several metrics. For example for the case of distributional outcomes, the Wasserstein metric is popular and easy to handle for one-dimensional distributions but it is very tedious to apply it for multivariate distributions (Torous et al., 2024) and alternative metrics that are easier to implement for multivariate distributions such as the Fisher-Rao metric or sliced Wasserstein metric (Bonneel et al., 2015) may sometimes be preferable. There are also many metrics available for the space of symmetric positive-definite matrices and the space of networks. The specific choice of metric could have a bearing on the results of a causal analysis. Metric selection in general and especially in a causal context remains an open problem (Dubey et al., 2024).

Furthermore, it is clearly important to further develop approaches for inference and uncertainty quantification for synthetic control models and their generalizations. One possibility to create an appropriate asymptotic framework is to extend the results of Chernozhukov et al. (2021a,b). Another promising avenue for future research is to extend the geodesic synthetic control model to the case of a staggered adoption setting (Ben-Michael et al., 2022).

7 Data Availability Statement

The data that support the findings of this study are openly available in the Research Institute of Economy, Trade and Industry (RIETI) at <https://www.rieti.go.jp/jp/database/R-JIP2021/index.html>, the Human Fertility Database at www.humanfertility.org, and the Human Mortality Database at www.mortality.org.

References

Abadie, A. (2021) Using synthetic controls: Feasibility, data requirements, and methodological aspects. *Journal of Economic Literature*, **59**, 391–425.

Abadie, A., Diamond, A. and Hainmueller, J. (2010) Synthetic control methods for comparative case studies: Estimating the effect of California’s tobacco control program. *Journal of the American Statistical Association*, **105**, 493–505.

Abadie, A. and Gardeazabal, J. (2003) The economic costs of conflict: A case study of the Basque Country. *American Economic Review*, **93**, 113–132.

Abadie, A. and L’Hour, J. (2021) A penalized synthetic control estimator for disaggregated data. *Journal of the American Statistical Association*, **116**, 1817–1834.

Ambrosio, L., Gigli, N. and Savaré, G. (2008) *Gradient Flows in Metric Spaces and in the Space of Probability Measures*. Lectures in Mathematics. ETH Zürich. Birkhäuser Basel, 2nd edn.

Amjad, M., Shah, D. and Shen, D. (2018) Robust synthetic control. *Journal of Machine Learning Research*, **19**, 1–51.

Arkhangelsky, D., Athey, S., Hirshberg, D. A., Imbens, G. W. and Wager, S. (2021) Synthetic difference-in-differences. *American Economic Review*, **111**, 4088–4118.

Arnaudon, M., Barbaresco, F. and Yang, L. (2013) Riemannian medians and means with applications to radar signal processing. *IEEE Journal of Selected Topics in Signal Processing*, **7**, 595–604.

Arsigny, V., Fillard, P., Pennec, X. and Ayache, N. (2007) Geometric means in a novel vector space structure on symmetric positive-definite matrices. *SIAM Journal on Matrix Analysis and Applications*, **29**, 328–347.

Ben-Michael, E., Feller, A. and Rothstein, J. (2021) The augmented synthetic control method. *Journal of the American Statistical Association*, **116**, 1789–1803.

— (2022) Synthetic controls with staggered adoption. *Journal of the Royal Statistical Society Series B: Statistical Methodology*, **84**, 351–381.

Billera, L. J., Holmes, S. P. and Vogtmann, K. (2001) Geometry of the space of phylogenetic trees. *Advances in Applied Mathematics*, **27**, 733–767.

Bonneel, N., Rabin, J., Peyré, G. and Pfister, H. (2015) Sliced and Radon Wasserstein barycenters of measures. *Journal of Mathematical Imaging and Vision*, **51**, 22–45.

Bridson, M. R. and Haefliger, A. (1999) *Metric Spaces of Non-Positive Curvature*. Grundlehren der mathematischen Wissenschaften. Springer Berlin, Heidelberg.

Buss, S. R. and Fillmore, J. P. (2001) Spherical averages and applications to spherical splines and interpolation. *ACM Transactions on Graphics (TOG)*, **20**, 95–126.

Büttner, T. and Lutz, W. (1990) Estimating fertility responses to policy measures in the German Democratic Republic. *Population and Development Review*, **16**, 539–555.

Chen, K., Delicado, P. and Müller, H.-G. (2017) Modelling function-valued stochastic processes, with applications to fertility dynamics. *Journal of the Royal Statistical Society Series B: Statistical Methodology*, **79**, 177–196.

Chen, Y., Lin, Z. and Müller, H.-G. (2023a) Wasserstein regression. *Journal of the American Statistical Association*, **118**, 869–882.

Chen, Y., Zhou, Y., Chen, H., Gajardo, A., Fan, J., Zhong, Q., Dubey, P., Han, K., Bhattacharjee, S., Zhu, C., Iao, S. I., Kundu, P., Petersen, A. and Müller, H.-G. (2023b) *frechet: Statistical Analysis for Random Objects and Non-Euclidean Data*. URL: <https://CRAN.R-project.org/package=frechet>. R package version 0.3.0.

Cherian, A. and Sra, S. (2016) *Positive Definite Matrices: Data representation and Applications to Computer Vision*, 93–114. Cham: Springer. URL: https://doi.org/10.1007/978-3-319-45026-1_4.

Chernozhukov, V., Wüthrich, K. and Zhu, Y. (2021a) Distributional conformal prediction. *Proceedings of the National Academy of Sciences*, **118**, e2107794118.

— (2021b) An exact and robust conformal inference method for counterfactual and synthetic controls. *Journal of the American Statistical Association*, **116**, 1849–1864.

Dai, X., Lin, Z. and Müller, H.-G. (2021) Modeling sparse longitudinal data on Riemannian manifolds. *Biometrics*, **77**, 1328–1341.

Dryden, I. L., Koloydenko, A. and Zhou, D. (2009) Non-Euclidean statistics for covariance matrices, with applications to diffusion tensor imaging. *Annals of Applied Statistics*, **3**, 1102–1123.

Dubey, P., Chen, Y. and Müller, H.-G. (2024) Metric statistics: Exploration and inference for random objects with distance profiles. *Annals of Statistics*, **52**, 757–792.

Eltzner, B. and Huckemann, S. F. (2019) A smearsy central limit theorem for manifolds with application to high-dimensional spheres. *Annals of Statistics*, **47**, 3360–3381.

Ferman, B. and Pinto, C. (2021) Synthetic controls with imperfect pretreatment fit. *Quantitative Economics*, **12**, 1197–1221.

Fréchet, M. (1948) Les éléments aléatoires de nature quelconque dans un espace distancié. *Annales de l'Institut Henri Poincaré*, **10**, 215–310.

Ginestet, C. E., Simmons, A. and Kolaczyk, E. D. (2012) Weighted Fréchet means as convex combinations in metric spaces: properties and generalized median inequalities. *Statistics and Probability Letters*, **82**, 1859–1863.

Gunsilius, F., Hsieh, M. H. and Lee, M. J. (2024) Tangential Wasserstein projections. *Journal of Machine Learning Research*, **25**, 1–41.

Gunsilius, F. F. (2023) Distributional synthetic controls. *Econometrica*, **91**, 1105–1117.

Hsing, T. and Eubank, R. (2015) *Theoretical Foundations of Functional Data Analysis, with an Introduction to Linear Operators*, vol. 997. John Wiley & Sons.

Human Fertility Database (2025) Max Planck Institute for Demographic Research (Germany) and Vienna Institute of Demography (Austria). Available at www.humanfertility.org (data downloaded on March 16, 2025).

Human Mortality Database (2024) Max Planck Institute for Demographic Research (Germany), University of California, Berkeley (USA), and French Institute for Demographic Studies (France). Available at www.mortality.org (data downloaded on September 13, 2024).

Johnson, S. G. (2008) *The NLOpt nonlinear-optimization package*. URL: <https://github.com/stevengj/nlopt>.

Kolaczyk, E. D. and Csárdi, G. (2014) *Statistical Analysis of Network Data with R*, vol. 65. Springer New York.

Kurisu, D., Zhou, Y., Otsu, T. and Müller, H.-G. (2024) Geodesic causal inference. *arXiv preprint arXiv:2406.19604*.

Le, H. and Barden, D. (2014) On the measure of the cut locus of a Fréchet mean. *Bulletin of the London Mathematical Society*, **46**, 698–708.

Lin, Z. (2019) Riemannian geometry of symmetric positive definite matrices via Cholesky decomposition. *SIAM Journal on Matrix Analysis and Applications*, **40**, 1353–1370.

Lin, Z., Kong, D. and Wang, L. (2023) Causal inference on distribution functions. *Journal of the Royal Statistical Society Series B: Statistical Methodology*, **85**, 378–398.

Lin, Z. and Yao, F. (2019) Intrinsic Riemannian Functional data analysis. *Annals of Statistics*, **47**, 3533–3577.

McCann, R. J. (1997) A convexity principle for interacting gases. *Advances in Mathematics*, **128**, 153–179.

Notzon, F. C., Komarov, Y. M., Ermakov, S. P., Sempos, C. T., Marks, J. S. and Sempos, E. V. (1998) Causes of declining life expectancy in Russia. *JAMA*, **279**, 793–800.

Panaretos, V. M. and Zemel, Y. (2020) *An Invitation to Statistics in Wasserstein Space*. Springer New York.

Patrangenaru, V. and Ellingson, L. (2015) *Nonparametric Statistics on Manifolds and Their Applications to Object Data Analysis*. CRC Press.

Petersen, A. and Müller, H.-G. (2016) Functional data analysis for density functions by transformation to a Hilbert space. *Annals of Statistics*, **44**, 183–218.

Petersen, A. and Müller, H.-G. (2019) Fréchet regression for random objects with Euclidean predictors. *Annals of Statistics*, **47**, 691–719.

Petersen, A., Zhang, C. and Kokoszka, P. (2022) Modeling probability density functions as data objects. *Econometrics and Statistics*, **21**, 159–178.

Powell, M. J. D. (1994) *A Direct Search Optimization Method That Models the Objective and Constraint Functions by Linear Interpolation*, 51–67. Dordrecht: Springer Netherlands. URL: https://doi.org/10.1007/978-94-015-8330-5_4.

Ramsay, J. O. and Silverman, B. W. (2005) *Functional Data Analysis*. Springer Series in Statistics. Springer New York, 2nd edn.

Robbins, M. W., Saunders, J. and Kilmer, B. (2017) A framework for synthetic control methods with high-dimensional, micro-level data: Evaluating a neighborhood-specific crime intervention. *Journal of the American Statistical Association*, **112**, 109–126.

Scealy, J. and Welsh, A. (2011) Regression for compositional data by using distributions defined on the hypersphere. *Journal of the Royal Statistical Society Series B: Statistical Methodology*, **73**, 351–375.

Severn, K. E., Dryden, I. L. and Preston, S. P. (2022) Manifold valued data analysis of samples of networks, with applications in corpus linguistics. *Annals of Applied Statistics*, **16**, 368–390.

Stellato, B., Banjac, G., Goulart, P., Bemporad, A. and Boyd, S. (2020) OSQP: An operator splitting solver for quadratic programs. *Mathematical Programming Computation*, **12**, 637–672.

Sturm, K.-T. (2003) Probability measures on metric spaces of nonpositive curvature. *Heat Kernels and Analysis on Manifolds, Graphs, and Metric Spaces (Paris, 2002)*. *Contemp. Math.*, 338. Amer. Math. Soc., Providence, RI, **338**, 357–390.

Torous, W., Gunsilius, F. and Rigollet, P. (2024) An optimal transport approach to estimating causal effects via nonlinear difference-in-differences. *Journal of Causal Inference*, **12**, 20230004.

Van Dijcke, D. (2025) Regression discontinuity design with distribution-valued outcomes. *arXiv preprint arXiv:2504.03992*.

Wang, J.-L., Chiou, J.-M. and Müller, H.-G. (2016) Functional Data Analysis. *Annual Review of Statistics and its Application*, **3**, 257–295.

Yuan, Y., Zhu, H., Lin, W. and Marron, J. (2012) Local polynomial regression for symmetric positive definite matrices. *Journal of the Royal Statistical Society Series B: Statistical Methodology*, **74**, 697–719.

Zhou, Y., Kurisu, D., Otsu, T. and Müller, H.-G. (2025) Geodesic difference-in-differences. *arXiv:2501.17436*.

Zhou, Y. and Müller, H.-G. (2022) Network regression with graph Laplacians. *Journal of Machine Learning Research*, **23**, 1–41.

Zhu, C. and Müller, H.-G. (2023) Geodesic optimal transport regression. *arXiv preprint arXiv:2312.15376*.

SUPPLEMENTARY MATERIAL

S.1 Augmented Geodesic Synthetic Control Method

This section provides the formal development of the augmented geodesic synthetic control (GSC) method. While the main text offered the high-level motivation, here we present the assumptions explicitly, introduce the necessary geometric tools, and derive the estimator step by step.

The central idea behind the augmented GSC is to correct the potential bias of the standard GSC estimator by making use of geodesic transport maps (Zhu and Müller, 2023). These maps extend the displacement between two points in a metric space to any other point, thereby allowing synthetic predictions to be shifted consistently in accordance with regression adjustments. We formalize this notion in the following assumption.

Assumption S1. *Let (\mathcal{M}, d) be a unique geodesic space. For any two points $\alpha, \beta \in \mathcal{M}$, there exists a geodesic transport map $\Gamma_{\alpha, \beta} : \mathcal{M} \rightarrow \mathcal{M}$ such that:*

- (i) $\Gamma_{\alpha, \beta}(\alpha) = \beta$, i.e., the map sends the starting point α to the endpoint β ;
- (ii) for any $\omega \in \mathcal{M}$, there exists a unique $\zeta \in \mathcal{M}$ such that $\Gamma_{\alpha, \beta}(\omega) = \zeta$, i.e., the displacement from α to β can be consistently applied to any other point ω .

This assumption ensures that the geodesic segment connecting α and β can be “extended” from any other point $\omega \in \mathcal{M}$, producing a uniquely defined endpoint ζ . In other words, the direction and length of the geodesic from α to β induce a transformation that can be applied uniformly to all points in the space. In Euclidean space \mathbb{R}^q , this notion reduces to the familiar vector translation:

$$\Gamma_{\alpha, \beta}(\omega) = \omega + (\beta - \alpha),$$

so that each point ω is shifted by the same displacement vector that moves α to β . This construction extends naturally to general vector spaces, where geodesics correspond to

linear displacements, and to Riemannian manifolds, where it is realized through parallel transport along geodesics (Yuan et al., 2012; Lin and Yao, 2019; Chen et al., 2023a).

The concept of geodesic transport maps is broad and applies to many of the spaces considered in this paper, including networks, compositional data, covariance matrices, distributions, and functions; see Section S.1.1 for more detail.

Consider a metric space (\mathcal{M}_X, d_X) that may differ from (\mathcal{M}, d) and the corresponding data pairs $\{(\mathbf{Y}_{j,1:T}, \mathbf{X}_{j,1:T_0})\}_{1 \leq j \leq J+1}$, where $\mathbf{Y}_{j,1:s} = (Y_{j,1}, \dots, Y_{j,s}) \in \mathcal{M}^s$ and $\mathbf{X}_{j,1:s} = (X_{j,1}, \dots, X_{j,s}) \in \mathcal{M}_X^s$. Denote by $m_t(\mathbf{Z}_{j,1:T_0})$ a regression model aiming to predict $Y_{j,t}(N)$ for $t = T_0 + 1, \dots, T$, where $\mathbf{Z}_{j,1:T_0} = (\mathbf{Y}_{j,1:T_0}, \mathbf{X}_{j,1:T_0})$ and let $\hat{m}_t(\cdot)$ be its estimated version using data $\{(Y_{j,t}, \mathbf{Z}_{j,1:T_0})\}_{2 \leq j \leq J+1}$. Define

$$m_t^{(\bar{\mathbf{w}})}(\mathbf{Z}_{2:J+1,1:T_0}) = \arg \min_{\nu \in \mathcal{M}} \sum_{j=2}^{J+1} \bar{\mathbf{w}}_j d^2(\nu, m_t(\mathbf{Z}_{j,1:T_0})),$$

where $\bar{\mathbf{w}} \in \Delta^{J-1}$ is an optimal weight vector. Then the augmented GSC estimator is

$$\tau_t^{(\text{AGSC})} := \gamma_{Y_{1,t}^{(\text{AGSC})}, Y_{1,t}}^{(\text{GSC})}, \quad t = T_0 + 1, \dots, T,$$

where

$$Y_{1,t}^{(\text{AGSC})} = \Gamma_{\hat{m}_t^{(\bar{\mathbf{w}})}(\mathbf{Z}_{2:J+1,1:T_0}), \hat{m}_t(\mathbf{Z}_{1,1:T_0})}(Y_{1,t}^{(\text{GSC})}).$$

To see the rationale for this estimator, denote by $\mathcal{G}(\mathcal{M}) = \{\gamma_{\alpha,\beta} : \alpha, \beta \in \mathcal{M}\}$ the space of geodesics of the unique geodesic space \mathcal{M} . To compare geodesics, we define a binary relation \sim on $\mathcal{G}(\mathcal{M})$ through the geodesic transport map, where $\gamma_{\alpha_1,\beta_1} \sim \gamma_{\alpha_2,\beta_2}$ if and only if $\Gamma_{\alpha_1,\beta_1}(\omega) = \Gamma_{\alpha_2,\beta_2}(\omega)$ for all $\omega \in \mathcal{M}$. Indeed the binary relation \sim is an equivalence relation on $\mathcal{G}(\mathcal{M})$ (Zhou et al., 2025). If the geodesic $\gamma_{m_t^{(\bar{\mathbf{w}})}(\mathbf{Z}_{2:J+1,1:T_0}), m_t(\mathbf{Z}_{1,1:T_0})}$ serves as a substitute for the bias of the GSC estimator, the following result justifies the augmented GSC.

Proposition S1. *Under Assumption S1, suppose $\gamma_{m_t^{(\bar{\mathbf{w}})}(\mathbf{Z}_{2:J+1,1:T_0}), m_t(\mathbf{Z}_{1,1:T_0})} \sim \gamma_{Y_{1,t}^{(\text{GSC})}, Y_{1,t}(N)}$ for $t = T_0 + 1, \dots, T$. Then*

$$Y_{1,t}(N) = \Gamma_{m_t^{(\bar{\mathbf{w}})}(\mathbf{Z}_{2:J+1,1:T_0}), m_t(\mathbf{Z}_{1,1:T_0})}(Y_{1,t}^{(\text{GSC})}), \quad t = T_0 + 1, \dots, T.$$

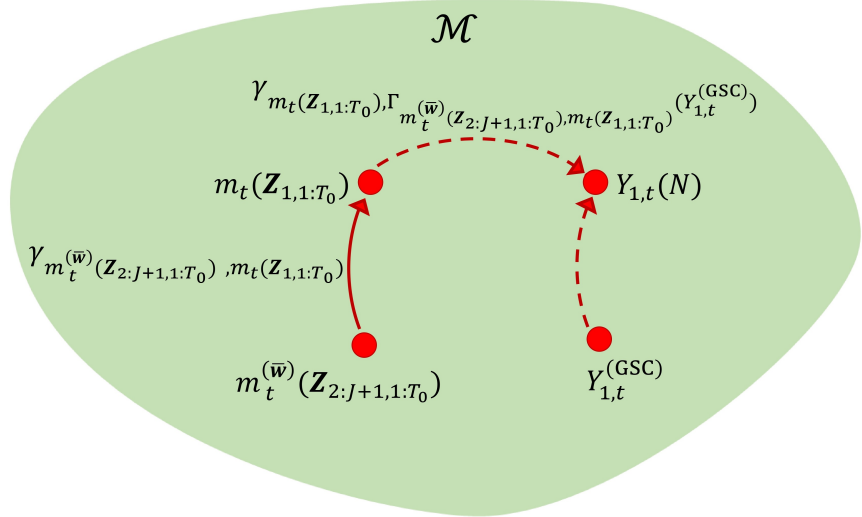


Figure S1: Illustration of the augmented geodesic synthetic control method. The circles symbolize random objects in the geodesic metric space \mathcal{M} and the arrows depict geodesics that connect the objects. The geodesic corresponding to the dashed red arrow from $Y_{1,t}^{(GSC)}$ to $Y_{1,t}(N)$ represents the bias of the geodesic synthetic control method in the setting considered in Section S.1. The solid red arrow represents the geodesic connecting $m_t^{(\bar{w})}(\mathbf{Z}_{2:J+1,1:T_0})$ and $m_t(\mathbf{Z}_{1,1:T_0})$ that serves as a substitute to assess the bias of the geodesic synthetic control estimator. The dashed red arrow from $m_t(\mathbf{Z}_{1,1:T_0})$ to $Y_{1,t}(N)$ represents the bias correction for the geodesic synthetic control estimator corresponding to the augmented geodesic control estimator.

Figure S1 illustrates the augmented GSC. For Euclidean outcomes, the augmented GSC estimator can be represented as

$$\begin{aligned}
Y_{1,t}^{(AGSC)} &= \underbrace{\sum_{j=2}^{J+1} \bar{w}_j Y_{j,t} + \hat{m}_t(\mathbf{Z}_{1,1:T_0})}_{=Y_{1,t}^{(GSC)}} - \underbrace{\sum_{j=2}^{J+1} \bar{w}_j \hat{m}_t(\mathbf{Z}_{j,1:T_0})}_{=\hat{m}_t^{(\bar{w})}(\mathbf{Z}_{2:J+1,1:T_0})} \\
&= \hat{m}_t(\mathbf{Z}_{1,1:T_0}) + \sum_{j=2}^{J+1} \bar{w}_j (Y_{j,t} - \hat{m}_t(\mathbf{Z}_{j,1:T_0})),
\end{aligned}$$

which coincides with the augmented SC estimator of Ben-Michael et al. (2021). Hence, the proposed augmented GSC estimator $Y_{1,t}^{(AGSC)}$ is a natural extension of the conventional augmented synthetic control estimator.

Remark S1 (*Regression estimator*). *To implement the augmented GSC with $X_{j,t} \in \mathcal{M}$, one can use the geodesic optimal transport regression (Zhu and Müller, 2023) to model*

$m_t(\mathbf{Z}_{j,1:T_0})$. For the special case where the covariates are Euclidean with $X_{j,t} \in \mathbb{R}^q$, employing global Fréchet regression (Petersen and Müller, 2019) is an option to implement $m_t(\mathbf{Z}_{j,1:T_0}) = m_t(\mathbf{X}_{j,1:T_0})$ in order to predict $Y_{j,t}(N)$ for $t = T_0 + 1, \dots, T$, as follows:

$$\hat{m}_t(\mathbf{x}) = \arg \min_{\nu \in \mathcal{M}} \frac{1}{J} \sum_{j=2}^{J+1} \{1 + (\mathbf{X}_{j,1:T_0} - \bar{\mathbf{X}}_{1:T_0})' \hat{\Sigma}_{1:T_0}^{-1} (\mathbf{x} - \bar{\mathbf{X}}_{1:T_0})\} d^2(\nu, Y_{j,t}),$$

where $\mathbf{X}_{j,1:T_0} = (X'_{j,1}, \dots, X'_{j,T_0})'$,

$$\bar{\mathbf{X}}_{1:T_0} = \frac{1}{J} \sum_{j=2}^{J+1} \mathbf{X}_{j,1:T_0}, \quad \hat{\Sigma}_{1:T_0} = \frac{1}{J} \sum_{j=2}^{J+1} (\mathbf{X}_{j,1:T_0} - \bar{\mathbf{X}}_{1:T_0})(\mathbf{X}_{j,1:T_0} - \bar{\mathbf{X}}_{1:T_0})'.$$

S.1.1 Examples of geodesic transport maps

We provide here specific geodesic transport maps that satisfy Assumption S1 for Examples 1–5 in Section 2. For the space of networks in Example 1, the geodesic corresponds to the line segment connecting the start and end points. Then the geodesic transport map is given as $\Gamma_{\alpha,\beta}(\omega) = \omega + (\beta - \alpha)$.

For the space of compositional data in Example 2, the geodesic transport map can be interpreted as a rotation of the point ω along the geodesic determined by α and β . The tangent vector for the geodesic $\gamma_{\alpha,\beta}$ is given by $v_{\alpha,\beta} = \beta - (\alpha' \beta) \alpha$, whose magnitude and direction encode the geodesic length and directionality needed to move from α to β along the sphere. The geodesic transport map is then defined as $\Gamma_{\alpha,\beta}(\omega) = \text{Exp}_{\omega}(\theta_{\alpha,\beta} v / \|v\|)$, where $\theta_{\alpha,\beta}$ is the angle between α and β , and $v = v_{\alpha,\beta} - (\omega' v_{\alpha,\beta}) \omega$ is the projection of $v_{\alpha,\beta}$ onto the tangent space at ω .

For the space of SPD matrices in Example 3, the geodesic transport map induced by the Frobenius metric is the line segment connecting two points. Then the geodesic transport map is $\Gamma_{\alpha,\beta}(\omega) = \omega + (\beta - \alpha)$. The geodesic transport map induced by the Log-Euclidean metric is $\Gamma_{\alpha,\beta}(\omega) = \exp\{\log \omega + (\log \beta - \log \alpha)\}$ and for the power metric family it is $\Gamma_{\alpha,\beta}(\omega) = [\omega^p + (\beta^p - \alpha^p)]^{1/p}$ where $p > 0$ is a constant denoting the power, $A^p = U \Lambda^p U'$ and $U \Lambda U'$ is the usual spectral decomposition of $A \in \text{Sym}_m^+$. Let \mathcal{L}_m^+ be the set of lower

triangular matrices with positive diagonal entries. For any $S \in \text{Sym}_m^+$, there exists a unique $L \in \mathcal{L}_m^+$ such that $S = LL'$ and a diffeomorphism \mathcal{L} between Sym_m^+ and \mathcal{L}_m^+ . For any $L \in \mathcal{L}_m^+$, let $\lfloor L \rfloor$ be the strictly lower triangular part and $\mathbb{D}(L)$ the diagonal part of L . For $\alpha, \beta, \omega \in \mathcal{L}_m^+$, the geodesic transport map induced by the Log-Cholesky metric is $\Gamma_{\alpha, \beta}(\omega) = \lfloor \omega \rfloor + (\lfloor \beta \rfloor - \lfloor \alpha \rfloor) + \exp \{ \log(\mathbb{D}(\omega)) + (\log(\mathbb{D}(\beta)) - \log(\mathbb{D}(\alpha))) \}$.

For the Wasserstein space in Example 4, the geodesic transport map is $\Gamma_{\alpha, \beta} = F_\beta^{-1} \circ F_\alpha$, where F_α and F_β^{-1} are the cumulative distribution function of the measure α and the quantile function of the measure β , respectively. The resulting endpoint of the geodesic $\gamma_{\omega, \zeta}$ is then $F_\zeta^{-1} = F_\beta^{-1} \circ F_\alpha \circ F_\omega^{-1}$ where F_ω^{-1} and F_ζ^{-1} denote the quantile functions of the measures ω and ζ .

For the space of functional data in Example 5, the geodesic transport map induced by the L^2 metric is the line segment connecting two points. Then the geodesic transport map is $\Gamma_{\alpha, \beta}(\omega) = \omega + (\beta - \alpha)$.

S.2 Geodesic Synthetic Difference-in-Differences

S.2.1 Construction of the estimator

We discuss an extension of synthetic difference-in-differences developed in [Arkhangelsky et al. \(2021\)](#) for the Euclidean case to outcomes located in geodesic metric spaces. Define

$$Y_{j, T_0+1:T}^{(\oplus)} = \arg \min_{\nu \in \mathcal{M}} \frac{1}{T - T_0} \sum_{t=T_0+1}^T d^2(\nu, Y_{j,t}), \quad j = 1, \dots, J+1,$$

$$Y_{1, T_0+1:T}^{(\oplus)}(D) = \arg \min_{\nu \in \mathcal{M}} \frac{1}{T - T_0} \sum_{t=T_0+1}^T d^2(\nu, Y_{1,t}(D)), \quad D \in \{N, I\}.$$

In what follows, the causal effect of interest is the geodesic τ from $Y_{1, T_0+1:T}^{(\oplus)}(N)$ to $Y_{1, T_0+1:T}^{(\oplus)}(I)$,

$$\tau = \gamma_{Y_{1, T_0+1:T}^{(\oplus)}(N), Y_{1, T_0+1:T}^{(\oplus)}(I)}.$$

Aiming at a geodesic synthetic difference-in-differences (GSDID) estimator, we introduce a vector of weights λ indexed by time in addition to the previously introduced

vector of weights \mathbf{w} indexed by units. For non-negative weight vectors in the simplex $\mathbf{w} \in \Delta^{J-1}$, $\boldsymbol{\lambda} \in \Delta^{T_0-1}$, $t = 1, \dots, T_0$, and $j = 1, \dots, J+1$, define

$$\begin{aligned} Y_{2:J+1,t}^{(\mathbf{w})} &= \arg \min_{\nu \in \mathcal{M}} \sum_{j=2}^{J+1} w_j d^2(\nu, Y_{j,t}), \quad Y_{j,1:T_0}^{(\boldsymbol{\lambda})} = \arg \min_{\nu \in \mathcal{M}} \sum_{t=1}^{T_0} \lambda_t d^2(\nu, Y_{j,t}), \\ Y_{2:J+1,1:T_0}^{(\mathbf{w}, \boldsymbol{\lambda})} &= \arg \min_{\nu \in \mathcal{M}} \sum_{j=2}^{J+1} w_j d^2(\nu, Y_{j,1:T_0}^{(\boldsymbol{\lambda})}), \quad Y_{2:J+1,T_0+1:T}^{(\mathbf{w}, \oplus)} = \arg \min_{\nu \in \mathcal{M}} \sum_{j=2}^{J+1} w_j d^2(\nu, Y_{j,T_0+1:T}^{(\oplus)}). \end{aligned}$$

With $\Gamma_{\alpha, \beta} : \mathcal{M} \rightarrow \mathcal{M}$ denoting a geodesic transport map for $\alpha, \beta \in \mathcal{M}$ as introduced in Assumption S1, we define the GSDID estimator for τ as

$$\tau^{(\text{GSDID})} = \gamma_{Y_{1,T_0+1:T}^{(\text{GSDID})}, Y_{1,T_0+1:T}^{(\oplus)}},$$

where

$$\begin{aligned} Y_{1,T_0+1:T}^{(\text{GSDID})} &= \Gamma_{Y_{2:J+1,1:T_0}^{(\overline{\mathbf{w}}, \overline{\boldsymbol{\lambda}})}, Y_{2:J+1,T_0+1:T}^{(\overline{\mathbf{w}}, \oplus)}} \left(Y_{1,1:T_0}^{(\overline{\boldsymbol{\lambda}})} \right), \\ \overline{\mathbf{w}} \in \arg \min_{\mathbf{w} \in \Delta^{J-1}} \frac{1}{T_0} \sum_{t=1}^{T_0} d^2(Y_{1,t}, Y_{2:J+1,t}^{(\mathbf{w})}), \quad \overline{\boldsymbol{\lambda}} \in \arg \min_{\boldsymbol{\lambda} \in \Delta^{T_0-1}} \frac{1}{J} \sum_{j=2}^{J+1} d^2(Y_{j,T_0+1:T}^{(\oplus)}, Y_{j,1:T_0}^{(\boldsymbol{\lambda})}). \end{aligned}$$

Note that for the special case of Euclidean outcomes, the proposed GSDID estimator becomes

$$\begin{aligned} Y_{1,T_0+1:T}^{(\text{GSDID})} &= Y_{1,1:T_0}^{(\overline{\boldsymbol{\lambda}})} + \left(Y_{2:J+1,T_0+1:T}^{(\overline{\mathbf{w}}, \oplus)} - Y_{2:J+1,1:T_0}^{(\overline{\mathbf{w}}, \overline{\boldsymbol{\lambda}})} \right) \\ &= \sum_{t=1}^{T_0} \overline{\boldsymbol{\lambda}}_t Y_{1,t} + \left(\frac{1}{T - T_0} \sum_{t=T_0+1}^T \sum_{j=2}^{J+1} \overline{w}_j Y_{j,t} - \sum_{t=1}^{T_0} \sum_{j=2}^{J+1} \overline{w}_j \overline{\boldsymbol{\lambda}}_t Y_{j,t} \right), \end{aligned}$$

which is the SDID estimator of [Arkhangelsky et al. \(2021\)](#). Thus, the proposed estimator is a natural extension of the established case with Euclidean outcomes. We discuss extensions to cases with multiple treated units or where the interest lies in the causal effects at multiple post-treatment time points in Remark S4 below.

Remark S2 (*Connection with geodesic synthetic control method and geodesic difference-in-differences*). *To discuss the relation of the proposed GSDID estimator with the GSC estimator introduced above and the geodesic DID (GDID) estimator introduced in [Zhou et al. \(2025\)](#), we note that GSC, GDID, and GSDID estimators can be represented as geodesic*

transports based on weighted averages of outcomes $\delta_{j,k}^{(M)}$, $k = 1, 2, 3$, using appropriate weights $w_j^{(M)}$, $M \in \{\text{GSC, GDID, GSDID}\}$, i.e.,

$$\tau^{(M)} := \gamma_{Y_{1,T_0+1:T}^{(M)}, Y_{1,T_0+1:T}^{(\oplus)}}$$

where

$$\begin{aligned} Y_{1,T_0+1:T}^{(M)} &= \Gamma_{\delta_{2:J+1,1:T_0}^{(M)}, \delta_{2:J+1,T_0+1:T}^{(M)}} \left(\delta_{1,1:T_0}^{(M)} \right), \quad \delta_{2:J+1,1:T_0}^{(M)} = \arg \min_{\nu \in \mathcal{M}} \sum_{j=2}^{J+1} w_j^{(M)} d^2(\nu, \delta_{j,1:T_0}^{(M)}), \\ \delta_{2:J+1,T_0+1:T}^{(M)} &= \arg \min_{\nu \in \mathcal{M}} \sum_{j=2}^{J+1} w_j^{(M)} d^2(\nu, \delta_{j,T_0+1:T}^{(M)}), \quad \delta_{1,1:T_0}^{(M)} = \arg \min_{\nu \in \mathcal{M}} \sum_{j=2}^{J+1} w_j^{(M)} d^2(\nu, \bar{\delta}_{j,1:T_0}^{(M)}), \end{aligned}$$

and

$$\begin{aligned} \{w_j^{(\text{GSC})}, \delta_{j,1:T_0}^{(\text{GSC})}, \delta_{j,T_0+1:T}^{(\text{GSC})}, \bar{\delta}_{j,1:T_0}^{(\text{GSC})}\} &= \{\bar{w}_j, Y_{j,1:T_0}^{(\oplus)}, Y_{j,T_0+1:T}^{(\oplus)}, Y_{1,1:T_0}^{(\oplus)}\}, \\ \{w_j^{(\text{GDID})}, \delta_{j,1:T_0}^{(\text{GDID})}, \delta_{j,T_0+1:T}^{(\text{GDID})}, \bar{\delta}_{j,1:T_0}^{(\text{GDID})}\} &= \left\{ \frac{1}{J}, Y_{j,1:T_0}^{(\oplus)}, Y_{j,T_0+1:T}^{(\oplus)}, Y_{1,1:T_0}^{(\oplus)} \right\}, \\ \{w_j^{(\text{GSDID})}, \delta_{j,1:T_0}^{(\text{GSDID})}, \delta_{j,T_0+1:T}^{(\text{GSDID})}, \bar{\delta}_{j,1:T_0}^{(\text{GSDID})}\} &= \{\bar{w}_j, Y_{j,1:T_0}^{(\bar{\lambda})}, Y_{j,T_0+1:T}^{(\bar{\lambda})}, Y_{1,1:T_0}^{(\bar{\lambda})}\}. \end{aligned}$$

Specifically, setting $T = T_0 + 1$ for the GSC and setting $T_0 = 1$, $T = 2$ for the GDID,

we have

$$Y_{1,T_0+1:T}^{(\text{GSC})} = \Gamma_{Y_{2:J+1,1:T_0}^{(\bar{w}, \oplus)}, Y_{2:J+1,T_0+1}^{(\bar{w})}} \left(Y_{2:J+1,1:T_0}^{(\bar{w}, \oplus)} \right) = Y_{2:J+1,T_0+1}^{(\bar{w})}, \quad (\text{S1})$$

$$Y_{1,T_0+1:T}^{(\text{GDID})} = \Gamma_{Y_{2:J+1,1}^{(\oplus)}, Y_{2:J+1,2}^{(\oplus)}} (Y_{1,1}), \quad (\text{S2})$$

where

$$Y_{2:J+1,t}^{(\oplus)} = \arg \min_{\nu \in \mathcal{M}} \frac{1}{J} \sum_{j=2}^{J+1} d^2(\nu, Y_{j,t}), \quad t = 1, 2.$$

The resulting estimators (S1) and (S2) coincide with the GSC and GDID estimators, respectively. Under Assumption S3 below, we have $Y_{1,T_0+1}^{(\text{GSC})} = Y_{1,T_0+1}(N)$. Comparing $\{\delta_{j,1:T_0}^{(\text{GSC})}, \bar{\delta}_{j,1:T_0}^{(\text{GSC})}\}$ and $\{\delta_{j,1:T_0}^{(\text{GSDID})}, \bar{\delta}_{j,1:T_0}^{(\text{GSDID})}\}$, the GSDID can be interpreted as attenuating the bias of the GSC estimator by introducing additional flexibility through the weights $\bar{\lambda}$ that are not present in the GSC. Under Assumption S4 below, we have $Y_{1,2}^{(\text{GDID})} = Y_{1,2}(N)$.

Comparing the weights $w_j^{(\text{GDID})}$ and $w_j^{(\text{GSDID})}$, GSDID can be seen as introducing additional flexibility to estimate the target $Y_{1,T_0+1:T}^{(\oplus)}(N)$ through the weights $\bar{\mathbf{w}}$, which may attenuate bias when the parallelity assumption does not hold. The proposed GSDID thus emerges as a method that combines favorable properties of both GSC and GDID.

S.2.2 Causal model for geodesic synthetic difference-in-differences

Consider the following model for potential outcomes without intervention:

$$Y_{j,t}(N) = g(U_j, V_t), \quad t = 1, \dots, T, \quad j = 1, \dots, J+1, \quad (\text{S3})$$

where $(U_j, V_t) \in \mathcal{M} \times \mathcal{M}$ is a pair of unobservable characteristics of unit j at time t and $g(\cdot, \cdot) : \mathcal{M} \times \mathcal{M} \rightarrow \mathcal{M}$ is a measurable function, where \mathcal{M} is the geodesic metric space where the outcomes are located. Define

$$g^{(\oplus)}(U_j, V_{T_0+1:T}) = \arg \min_{\nu \in \mathcal{M}} \frac{1}{T - T_0} \sum_{t=T_0+1}^T d^2(\nu, g(U_j, V_t)).$$

For non-negative weight vectors in the simplex $\mathbf{w} \in \Delta^{J-1}$ and $\boldsymbol{\lambda} \in \Delta^{T_0-1}$, we additionally define

$$\begin{aligned} g^{(\boldsymbol{\lambda})}(U_j, V_{1:T_0}) &= \arg \min_{\nu \in \mathcal{M}} \sum_{t=1}^{T_0} \lambda_t d^2(\nu, g(U_j, V_t)), \\ g^{(\mathbf{w})}(U_{2:J+1}, V_t) &= \arg \min_{\nu \in \mathcal{M}} \sum_{j=2}^{J+1} w_j d^2(\nu, g(U_j, V_t)), \\ g^{(\mathbf{w}, \oplus)}(U_{2:J+1}, V_{T_0+1:T}) &= \arg \min_{\nu \in \mathcal{M}} \sum_{j=2}^{J+1} w_j d^2(\nu, g^{(\oplus)}(U_j, V_{T_0+1:T})), \\ g^{(\mathbf{w}, \boldsymbol{\lambda})}(U_{2:J+1}, V_{1:T_0}) &= \arg \min_{\nu \in \mathcal{M}} \sum_{j=2}^{J+1} w_j d^2(\nu, g^{(\boldsymbol{\lambda})}(U_j, V_{1:T_0})). \end{aligned}$$

We impose the following assumptions.

Assumption S2. For any $\mathbf{w} \in \Delta^{J-1}$ and $\boldsymbol{\lambda} \in \Delta^{T_0-1}$, weighted Fréchet means $g^{(\boldsymbol{\lambda})}(U_j, V_{1:T_0})$, $g^{(\oplus)}(U_j, V_{T_0+1:T})$, $g^{(\mathbf{w})}(U_{2:J+1}, V_t)$, $g^{(\mathbf{w}, \oplus)}(U_{2:J+1}, V_{T_0+1:T})$, and $g^{(\mathbf{w}, \boldsymbol{\lambda})}(U_{2:J+1}, V_{1:T_0})$ exist and are unique.

For $t = 1, \dots, T_0$ and $j = 1, \dots, J+1$, define

$$\mathbb{W}_t^* = \left\{ \mathbf{w}^* \in \Delta^{J-1} : d(g(U_1, V_t), g^{(\mathbf{w}^*)}(U_{2:J+1}, V_t)) = \inf_{\mathbf{w} \in \Delta^{J-1}} d(g(U_1, V_t), g^{(\mathbf{w})}(U_{2:J+1}, V_t)) \right\},$$

and

$$\begin{aligned} \Lambda_j^* &= \left\{ \boldsymbol{\lambda}^* \in \Delta^{T_0-1} : d(g^{(\oplus)}(U_j, V_{T_0+1:T}), g^{(\boldsymbol{\lambda}^*)}(U_j, V_{1:T_0})) \right. \\ &\quad \left. = \inf_{\boldsymbol{\lambda} \in \Delta^{T_0-1}} d(g^{(\oplus)}(U_j, V_{T_0+1:T}), g^{(\boldsymbol{\lambda})}(U_j, V_{1:T_0})) \right\}. \end{aligned}$$

Assumption S3 (Synthetic control).

(i) For $t = 1, \dots, T_0$, $\mathbb{W}_t^* = \{ \mathbf{w} \in \Delta^{J-1} : d(g(U_1, V_t), g^{(\mathbf{w})}(U_{2:J+1}, V_t)) = 0 \}$ and $\bigcap_{t=1}^{T_0} \mathbb{W}_t^*$ is not empty.

(ii) The set $\bigcap_{j=2}^{J+1} \Lambda_j^*$ is not empty. For any $\boldsymbol{\lambda} \in \bigcap_{j=2}^{J+1} \Lambda_j^*$, $\bigcap_{t=1}^{T_0} \mathbb{W}_t^* \subset \mathbb{W}_{\boldsymbol{\lambda}}^* \cap \mathbb{W}_{\oplus}^*$ where

$$\mathbb{W}_{\boldsymbol{\lambda}}^* = \left\{ \mathbf{w} \in \Delta^{J-1} : d(g^{(\boldsymbol{\lambda})}(U_1, V_{1:T_0}), g^{(\mathbf{w}, \boldsymbol{\lambda})}(U_{2:J+1}, V_{1:T_0})) = 0 \right\},$$

$$\mathbb{W}_{\oplus}^* = \left\{ \mathbf{w} \in \Delta^{J-1} : d(g^{(\oplus)}(U_1, V_{T_0+1:T}), g^{(\mathbf{w}, \oplus)}(U_{2:J+1}, V_{T_0+1:T})) = 0 \right\}.$$

Assumption S4 (Parallel trend).

(i) The set $\bigcap_{j=2}^{J+1} \Lambda_j^*$ is not empty and $\bigcap_{j=2}^{J+1} \Lambda_j^* \subset \Lambda_1^*$.

(ii) The set $\bigcap_{t=1}^{T_0} \mathbb{W}_t^*$ is not empty. For any $\mathbf{w} \in \bigcap_{t=1}^{T_0} \mathbb{W}_t^*$, $\boldsymbol{\lambda}_2 \in \bigcap_{j=2}^{J+1} \Lambda_j^*$ and $\boldsymbol{\lambda}_1 \in \Lambda_1^*$,

$$\Gamma_{\alpha, \beta} (g^{(\boldsymbol{\lambda}_1)}(U_1, V_{1:T_0})) = g^{(\oplus)}(U_1, V_{T_0+1:T}),$$

where $\alpha = g^{(\mathbf{w}, \boldsymbol{\lambda}_2)}(U_{2:J+1}, V_{1:T_0})$ and $\beta = g^{(\mathbf{w}, \oplus)}(U_{2:J+1}, V_{T_0+1:T})$.

Assumption S3 is for the GSC. Assumption S3(ii) implies that the optimal weights \mathbf{w} such that $Y_{2:J+1,t}^{(\mathbf{w})} = Y_{1,t}(N)$ at each time point $t = 1, \dots, T_0$ are still optimal in the sense that $Y_{1,1:T_0}^{(\boldsymbol{\lambda})}(N)$ and $Y_{1,T_0+1:T}^{(\oplus)}(N)$ respectively coincide with $Y_{2:J+1,1:T_0}^{(\mathbf{w}, \boldsymbol{\lambda})}(N)$ and $Y_{2:J+1,T_0+1:T}^{(\mathbf{w}, \oplus)}(N)$ as long as $\boldsymbol{\lambda}$ belongs to the set of optimal weights $\bigcap_{j=2}^{J+1} \Lambda_j^*$ such that for $j = 2, \dots, J+1$, $Y_{j,1:T_0}^{(\boldsymbol{\lambda})}$ is the closest to $Y_{j,T_0+1:T}^{(\oplus)}(N)$ with respect to the metric d among the

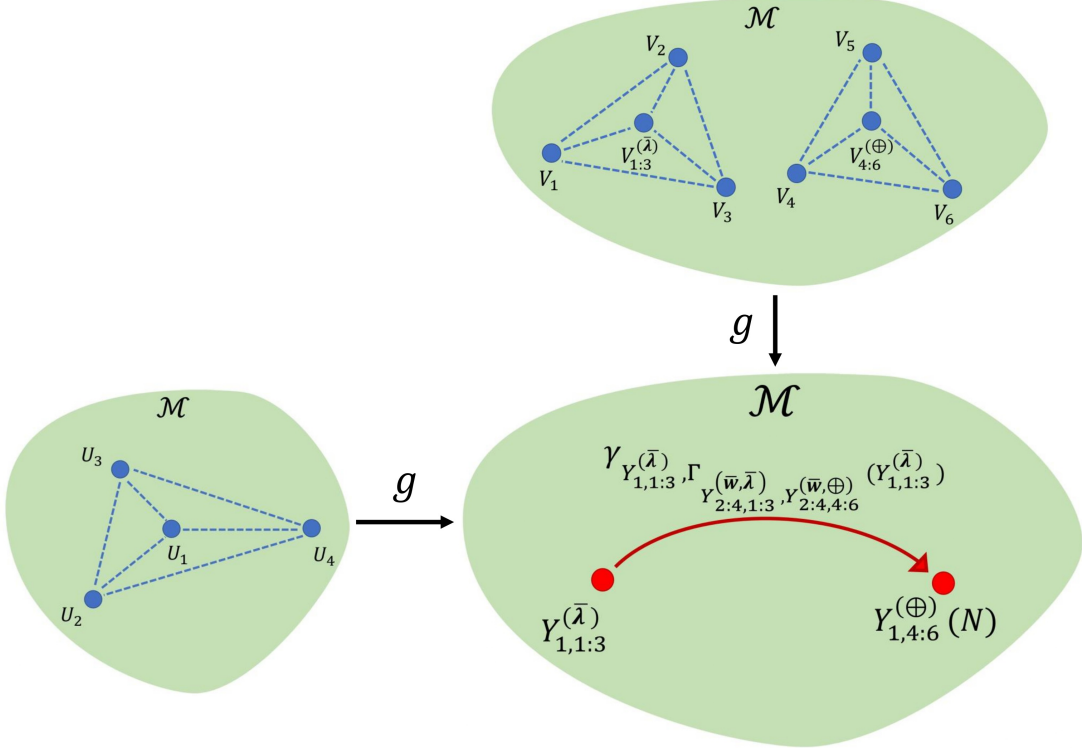


Figure S2: Illustration of geodesic synthetic difference-in-differences under Assumption S3. The circles symbolize objects in the geodesic metric space \mathcal{M} . Under Assumption S3, $Y_{2:4,1:3}^{(\bar{w}, \bar{\lambda})} = Y_{1,1:3}^{(\bar{\lambda})}$ and $Y_{2:4,4:6}^{(\bar{w}, \oplus)} = Y_{1,4:6}^{(\oplus)}$. The solid red arrow is the geodesic from $Y_{1,1:3}^{(\bar{\lambda})}$ to $Y_{1,4:6}^{(\oplus)}(N)$, representing the bias correction for geodesic synthetic controls as effected by geodesic synthetic difference-in-differences.

Fréchet means $Y_{j,1:T_0}^{(\lambda_0)}$ with $\lambda_0 \in \Delta^{T_0-1}$. Figure S2 illustrates the GSDID under Assumption S3.

Assumption S4(ii) corresponds to the parallel trend assumption for the GDID. We refer to Zhou et al. (2025) for more details about its construction and theoretical properties. For Euclidean outcomes, Assumption S4(ii) reduces to

$$g^{(\lambda_1)}(U_1, V_{1:T_0}) + \{g^{(w, \oplus)}(U_{2:J+1}, V_{T_0+1:T}) - g^{(w, \lambda_2)}(U_{2:J+1}, V_{1:T_0})\} = g^{(\oplus)}(U_1, V_{T_0+1:T}),$$

which corresponds to the standard assumption of parallel trends in the canonical DID framework (Zhou et al., 2025). Figure S3 illustrates the GSDID under Assumption S4.

For the space of networks (Example 1), Wasserstein space (Example 4), the space of functional data (Example 5), and the space of SPD matrices (Example 3) with either the

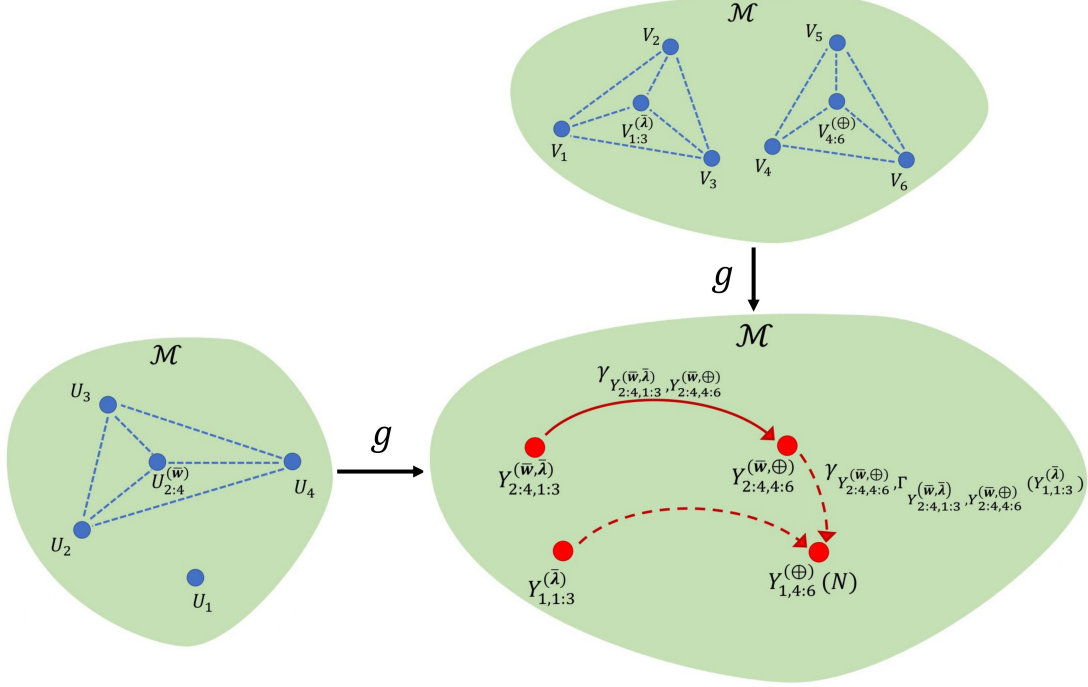


Figure S3: Illustration of GSDID under Assumption S4. The circles symbolize objects in the geodesic metric space \mathcal{M} . Arrows depict geodesics connecting them. The dashed red arrow from $Y_{1,1:3}^{(\bar{\lambda})}$ to $Y_{1,4:6}^{(\oplus)}(N)$ represents the trend between pre-treatment and post-treatment for unit 1. The solid red arrow represents the parallel trend. The dashed red arrow from $Y_{2:4,4:6}^{(\bar{w}, \oplus)}$ to $Y_{1,4:6}^{(\oplus)}(N)$ represents the bias correction of the GSC affected by the GSDID.

Frobenius metric, the power metric family, the Log-Euclidean metric or the Log-Cholesky metric, one can verify Assumptions S2, S3, and S4(i). Indeed, letting $g(U_j, V_t) = \gamma_{U_j, V_t}(\alpha)$, $\alpha \in (0, 1)$,

$$g^{(\mathbf{w}, \lambda)}(U_{2:J+1}, V_{1:T_0}) = \gamma_{U_{2:J+1}^{(\mathbf{w})}, V_{1:T_0}^{(\lambda)}}(\alpha), \quad g^{(\mathbf{w}, \oplus)}(U_{2:J+1}, V_{T_0+1:T}) = \gamma_{U_{2:J+1}^{(\mathbf{w})}, V_{T_0+1:T}^{(\oplus)}}(\alpha)$$

for any $\mathbf{w} \in \Delta^{J-1}$ and any $\lambda \in \Delta^{T_0-1}$, where

$$U_{2:J+1}^{(\mathbf{w})} = \arg \min_{\nu \in \mathcal{M}} \sum_{j=2}^{J+1} w_j d^2(\nu, U_j),$$

$$V_{T_0+1:T}^{(\oplus)} = \arg \min_{\nu \in \mathcal{M}} \frac{1}{T - T_0} \sum_{t=T_0+1}^T d^2(\nu, V_t), \quad V_{1:T_0}^{(\lambda)} \in \arg \min_{\nu \in \mathcal{M}} \sum_{t=1}^{T_0} \lambda_t d^2(\nu, V_t).$$

For the space of compositional data (Example 2), consider the causal model $g(U_j, V_t) =$

$\text{Exp}_{V_t}(\text{Log}_{U_1}(U_j))$. If we additionally assume that

$$g^{(\lambda)}(U_j, V_{1:T_0}) = \text{Exp}_{V_{1:T_0}^{(\lambda)}}(\text{Log}_{U_1}(U_j)), \quad g^{(\oplus)}(U_j, V_{T_0+1:T}) = \text{Exp}_{V_{T_0+1:T}^{(\oplus)}}(\text{Log}_{U_1}(U_j))$$

for any $j = 1, \dots, J+1$ and any $\lambda \in \Delta^{T_0-1}$, Assumptions [S2](#), [S3](#), and [S4\(i\)](#) can be verified.

The following result establishes the identification of the GSDID estimator.

Theorem S1. *Suppose that Assumptions [S1](#) and [S2](#) hold for the model [\(S3\)](#). Then under Assumption [S3](#) or [S4](#), we have*

$$Y_{1,T_0+1:T}^{(\text{GSDID})} = Y_{1,T_0+1:T}^{(\oplus)}(N). \quad (\text{S4})$$

Theorem [S1](#) provides a type of double robustness property of the GSDID estimator. Specifically, even if the weights \bar{w} for GSC or $\bar{\lambda}$ for GDID fail to remove the bias of the method, the combination of weights can compensate for this. This double robustness property corresponds to the double robustness property of synthetic DID for Euclidean outcomes and is similar to the property of the augmented inverse probability weighting estimator for Euclidean outcomes, demonstrating the possibility of trading off the accuracy of the outcome model and the treatment assignment model. We refer to [Kurisu et al. \(2024\)](#) for further discussion of the augmented inverse probability weighting estimator and its double robustness for outcomes taking values in geodesic metric spaces.

Remark S3 (Placebo permutation test). *We can also employ a placebo permutation test for GSDID. We first compute $Y_{j,T_0+1:T}^{(\text{GSDID})}$ for $j = 2, \dots, J+1$ by applying the same algorithm to obtain $Y_{1,T_0+1:T}^{(\text{GSDID})}$ by pretending the treated unit is j . The p -value for the null hypothesis of no causal effect by the intervention to unit $j = 1$ is given by*

$$\frac{\text{rank of } d(Y_{1,T_0+1:T}^{(\oplus)}, Y_{1,T_0+1:T}^{(\text{GSDID})}) \text{ in } \{d(Y_{j,T_0+1:T}^{(\oplus)}, Y_{j,T_0+1:T}^{(\text{GSDID})}) : j = 1, \dots, J+1\}}{J+1}.$$

Remark S4 (Extensions). *The GSDID estimator can be extended in several directions.*

First, if one is interested in causal effects at different time points, one can replace $Y_{2:J+1,1:T_0}^{(\bar{w}, \bar{\lambda})}$

and $Y_{1,1:T_0}^{(\bar{\lambda})}$ in the definition of $Y_{1,T_0+1:T}^{(\text{GSDID})}$ with $Y_{2:J+1,1:T_0}^{(\bar{w}, \bar{\lambda}_t)}$ and $Y_{1,1:T_0}^{(\bar{\lambda}_t)}$, respectively, where

$$\bar{\lambda}_t \in \arg \min_{\lambda \in \Delta^{T_0-1}} \frac{1}{J} \sum_{j=2}^{J+1} d^2(Y_{j,t}, Y_{j,1:T_0}^{(\lambda)}), \quad t = T_0 + 1, \dots, T.$$

In this case, the causal effects of interest are given by $\gamma_{Y_{1,t}(N), Y_{1,t}(I)}$ for $t = T_0 + 1, \dots, T$.

Second, if there are multiple treated units, say $\{(Y_{11,t}, \dots, Y_{1K,t})\}_{t=1}^T$ instead of $\{Y_{1,t}\}_{t=1}^T$, one can replace $Y_{1,1:T_0}^{(\bar{\lambda})}$ in the definition of $Y_{1,T_0+1:T}^{(\text{GSDID})}$ with $Y_{1,1:K,1:T_0}^{(\bar{\lambda}, \oplus)}$ for the implementation of the GSDID, where

$$Y_{1,1:K,1:T_0}^{(\lambda, \oplus)} = \arg \min_{\nu \in \mathcal{M}} \sum_{t=1}^{T_0} \lambda_t d^2(\nu, Y_{1,1:K,t}^{(\oplus)}), \quad Y_{1,1:K,t}^{(\oplus)} = \arg \min_{\nu \in \mathcal{M}} \frac{1}{K} \sum_{j=1}^K d^2(\nu, Y_{1j,t}).$$

If $Y_{1j,t}(I)$ and $Y_{1j,t}(N)$ denote potential outcomes of the j -th treated unit at time t with and without intervention, respectively, the causal effect of interest is given by

$$\gamma_{Y_{1,1:K,T_0+1:T}^{(\oplus, \oplus)}(N), Y_{1,1:K,T_0+1:T}^{(\oplus, \oplus)}(I)},$$

where

$$Y_{1,1:K,T_0+1:T}^{(\oplus, \oplus)}(D) = \arg \min_{\nu \in \mathcal{M}} \frac{1}{T - T_0} \sum_{t=T_0+1}^T d^2(\nu, Y_{1,1:K,t}^{(\oplus)}(D)), \quad D \in \{N, I\},$$

$$Y_{1,1:K,t}^{(\oplus)}(D) = \arg \min_{\nu \in \mathcal{M}} \frac{1}{K} \sum_{j=1}^K d^2(\nu, Y_{1j,t}(N)).$$

Third, if one is interested in causal effects at different time points with multiple treated units, one can replace $Y_{1,1:T_0}^{(\bar{\lambda})}$ in the definition of $Y_{1,T_0+1:T}^{(\text{GSDID})}$ with $Y_{1,1:K,1:T_0}^{(\bar{\lambda}_t, \oplus)}$. In this case, the causal effects of interest are given by

$$\gamma_{Y_{1,1:K,t}^{(\oplus)}(N), Y_{1,1:K,t}^{(\oplus)}(I)}, \quad t = T_0 + 1, \dots, T.$$

By appropriately modifying Assumptions [S2–S4](#), it is also possible to extend Theorem [S1](#) to the case with multiple treated units. Further combinations of times and treated units are possible and can be handled analogously.

S.2.3 Analysis of the effect of the collapse of the Soviet Union on mortality with geodesic synthetic difference-in-differences

The collapse of the Soviet Union in 1991 led to severe economic and social disruptions, profoundly affecting mortality patterns in Russia. The transition from a centrally planned economy to a market-based system was marked by economic instability, rising unemployment, healthcare system deterioration, and increased alcohol consumption, all of which contributed to a dramatic decline in life expectancy. Between 1990 and 1994, life expectancy for Russian men fell from 63.8 to 57.6 years, while for women, it declined from 74.4 to 71.0 years (Notzon et al., 1998). Rather than relying solely on summary measures such as life expectancy, a more comprehensive understanding of this demographic shock requires a more detailed analysis, which motivates the analysis of entire age-at-death distributions.

The data supporting such an analysis is available from the [Human Mortality Database](#), which provides life tables with 5-year time intervals for multiple countries, including Russia and various Western European countries. These life tables are sorted by age and calendar year and can easily be converted into age-at-death distributions. Specifically, for each country, we obtain age-at-death distributions by constructing their probability densities through slightly smoothing the histograms of the age-at-death distribution obtained from the available life table data. For this preprocessing step we use the `CreateDensity` function from the `frechet` package (Chen et al., 2023b).

We treat Russia as the intervention unit, while the control group consists of 19 Western European countries: Austria, Belgium, Denmark, Finland, France, Germany, Greece, Iceland, Ireland, Italy, Luxembourg, Netherlands, Norway, Portugal, Slovenia, Spain, Sweden, Switzerland, and the United Kingdom. For this analysis, we apply the geodesic synthetic difference-in-differences model (GSDID) as delineated in Sections S.2.1 and S.2.2. to estimate the causal effect of the Soviet Union's collapse on Russia's age-at-death distribution

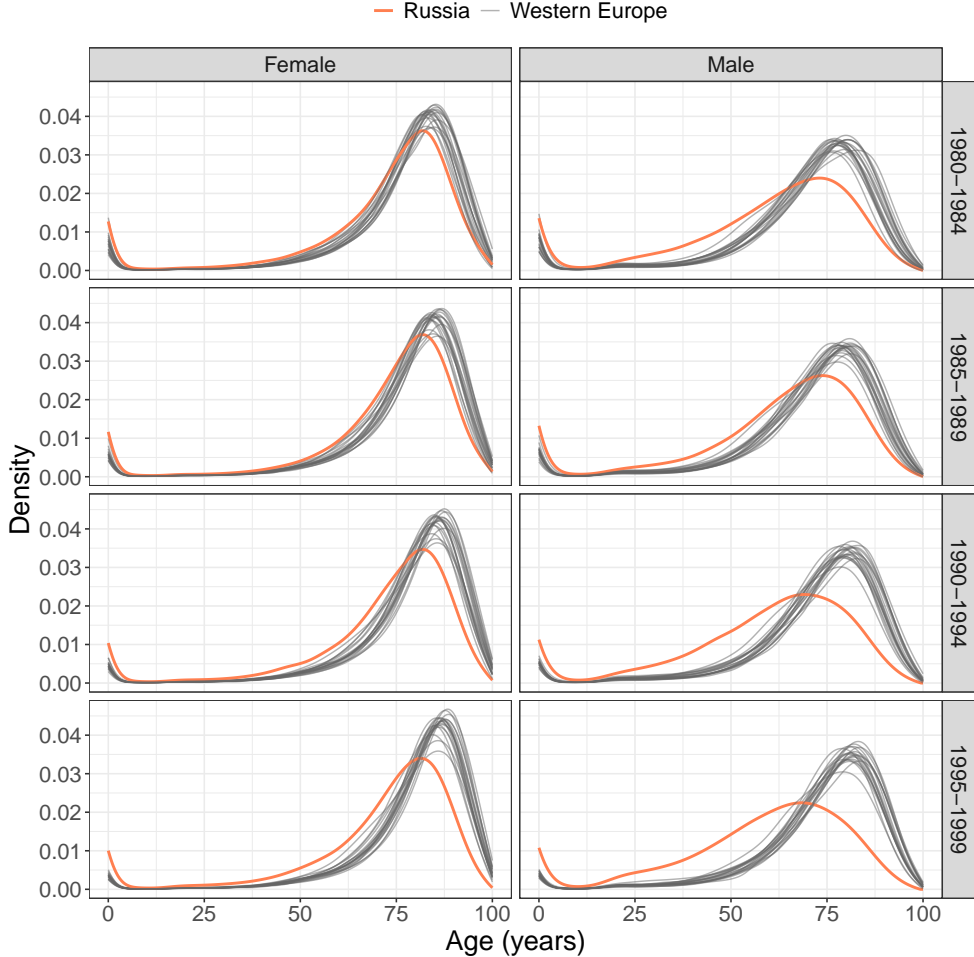


Figure S4: Estimated probability densities for age-at-death distributions of females (left) and males (right) for Russia (red) and Western European countries (grey) for the calendar periods 1980–1984, 1985–1989, 1990–1994, and 1995–1999.

using the Wasserstein metric (see Example 4).

Details on the implementation of GSDID are in Algorithm S1. The optimization problems in Steps 1 and 2 of Algorithm S1 are addressed in a similar way to those in Step 1 of Algorithm 1. The third step of Algorithm S1 involves constructing the geodesic transport map, with details provided in Section S.1.1.

We consider four time periods: 1980–1984 and 1985–1989 as pre-treatment periods, and 1990–1994 and 1995–1999 as post-treatment periods, with the Soviet collapse occurring in 1991. The effects of the collapse are expected to be extended over time. Figure S4 illustrates the available data through the estimated probability densities of the age-at-

Algorithm S1: Geodesic Synthetic Difference-in-Differences

Input: data $\{Y_{j,t} : j = 1, \dots, J+1, t = 1, \dots, T\}$.

Output: geodesic synthetic difference-in-differences estimator $\tau^{(\text{GSDID})}$.

1 $\bar{\mathbf{w}} = (\bar{w}_2, \dots, \bar{w}_{J+1}) \leftarrow$ the estimated unit weights:

$$\bar{\mathbf{w}} \in \arg \min_{\mathbf{w} \in \Delta^{J-1}} \frac{1}{T_0} \sum_{t=1}^{T_0} d^2(Y_{1,t}, Y_{2:J+1,t}^{(\mathbf{w})}),$$

where $Y_{2:J+1,t}^{(\mathbf{w})} = \arg \min_{\nu \in \mathcal{M}} \sum_{j=2}^{J+1} w_j d^2(\nu, Y_{j,t})$ for $t = 1, \dots, T_0$;

2 $\bar{\boldsymbol{\lambda}} = (\bar{\lambda}_1, \dots, \bar{\lambda}_{T_0}) \leftarrow$ the estimated time weights:

$$\bar{\boldsymbol{\lambda}} = \arg \min_{\boldsymbol{\lambda} \in \Delta^{T_0-1}} \frac{1}{J} \sum_{j=2}^{J+1} d^2(Y_{j,T_0+1:T}^{(\oplus)}, Y_{j,1:T_0}^{(\boldsymbol{\lambda})}),$$

where

$$Y_{j,T_0+1:T}^{(\oplus)} = \arg \min_{\nu \in \mathcal{M}} \frac{1}{T - T_0} \sum_{t=T_0+1}^T d^2(\nu, Y_{j,t}),$$

$$Y_{j,1:T_0}^{(\boldsymbol{\lambda})} = \arg \min_{\nu \in \mathcal{M}} \sum_{t=1}^{T_0} \lambda_t d^2(\nu, Y_{j,t})$$

for $j = 1, \dots, J+1$;

3 $Y_{1,T_0+1:T}^{(\text{GSDID})} = \Gamma_{Y_{2:J+1,1:T_0}^{(\bar{\mathbf{w}}, \bar{\boldsymbol{\lambda}})}, Y_{2:J+1,T_0+1:T}^{(\bar{\mathbf{w}}, \oplus)}} \left(Y_{1,1:T_0}^{(\bar{\boldsymbol{\lambda}})} \right) \leftarrow$ the synthetic difference-in-differences unit, where

$$Y_{2:J+1,1:T_0}^{(\bar{\mathbf{w}}, \bar{\boldsymbol{\lambda}})} = \arg \min_{\nu \in \mathcal{M}} \sum_{j=2}^{J+1} \bar{w}_j d^2(\nu, Y_{j,1:T_0}^{(\bar{\boldsymbol{\lambda}})}),$$

$$Y_{2:J+1,T_0+1:T}^{(\bar{\mathbf{w}}, \oplus)} = \arg \min_{\nu \in \mathcal{M}} \sum_{j=2}^{J+1} \bar{w}_j d^2(\nu, Y_{j,T_0+1:T}^{(\oplus)});$$

4 $\tau^{(\text{GSDID})} = \gamma_{Y_{1,T_0+1:T}^{(\text{GSDID})}, Y_{1,T_0+1:T}^{(\oplus)}} \leftarrow$ the geodesic synthetic difference-in-differences estimator.

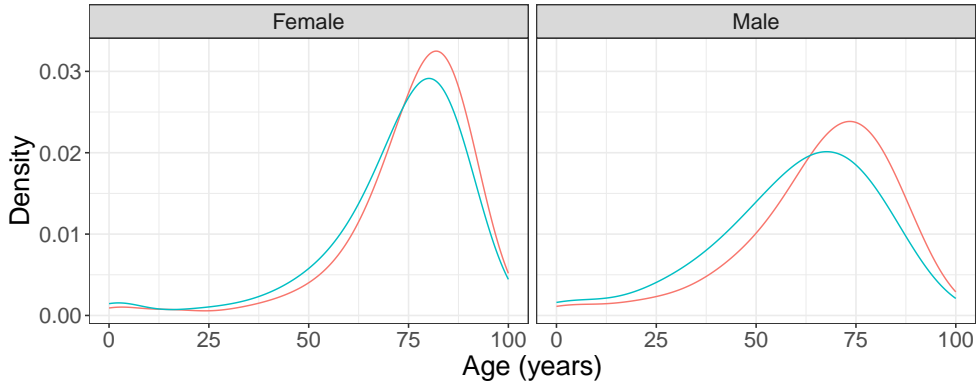


Figure S5: Geodesic synthetic difference-in-differences estimator for age-at-death distributions in Russia, shown separately for females (left) and males (right). The red curves represent the age-at-death density for the synthetic difference-in-differences unit, while the blue curves represent the average post-treatment age-at-death density for Russia.

death distributions for males and females in Russia and the control countries. In Russia, a clear leftward shift is observed in the post-treatment periods (1990–1994 and 1995–1999), indicating increased mortality and a decline in longevity. This shift is especially pronounced for males, reflecting a substantial reduction in survival probabilities at younger and middle ages.

When applying GSDID, we reweigh the control countries to ensure that their pre-treatment time trends align with those of Russia, allowing for a difference-in-differences analysis within the geodesic framework. Figure S5 presents the observed and synthetic post-treatment age-at-death densities for both males and females. The GSDID framework captures not only the overall reduction in life expectancy but also the complex age- and gender-specific effects of the economic and societal shocks that resulted from the collapse of the Soviet Union. The results confirm that the collapse caused a significant leftward shift in Russia’s age-at-death distribution, with sharply increased mortality risk across multiple age groups. The effect was particularly severe for males, reflected in a more pronounced leftward shift. A plausible explanation for this gender disparity is the heightened vulnerability of working-age men to economic collapse, labor market instability and increased alcohol-related mortality.

To assess the statistical significance of this effect, we apply the placebo permutation test described in Remark S3. This procedure constructs synthetic age-at-death distributions for each control country by pretending it was treated, allowing us to evaluate whether the observed shift in Russia’s mortality patterns is extreme compared to placebo assignments. The resulting p -values for the null hypothesis of no causal effect are 0 for both females and males. These findings provide strong evidence that the collapse of the Soviet Union indeed caused a substantial and statistically significant impact on mortality for nearly all age groups in Russia.

S.3 Optimization Details

This section provides additional computational details for the implementation of geodesic synthetic control (GSC) and geodesic synthetic difference-in-differences (GSDID) estimators. We present explicit formulations of the optimization problems, describe how weighted Fréchet means are computed in different geodesic metric spaces, and discuss the solver strategies adopted in each case.

S.3.1 Unit and time weights

Both GSC and GSDID rely on optimizing weights attached to observational indices rather than features of the objects themselves. Specifically, the *unit weights* $\bar{\mathbf{w}} \in \Delta^{J-1}$ form convex combinations of control units, while the *time weights* $\bar{\boldsymbol{\lambda}} \in \Delta^{T_0-1}$ form convex combinations of pre-treatment periods. Random objects are then averaged via weighted Fréchet means in the respective metric space. Thus, the weights govern the influence of units or time periods but do not vary across internal coordinates of the objects (such as quantiles of a distribution). This mirrors the SDID construction and preserves interpretability in the geodesic extension.

S.3.2 General optimization problems

The estimation of unit and time weights in GSC and GSDID is formulated as minimization problems involving distances between the treated unit and weighted Fréchet means of control units.

For the GSC estimator, only unit weights are involved. Specifically, the unit weights $\bar{\mathbf{w}} \in \Delta^{J-1}$ are chosen to minimize the average squared distance between the treated outcome $Y_{1,t}$ and the synthetic control outcome $Y_{2:J+1,t}^{(\mathbf{w})}$ over the pre-treatment period,

$$\bar{\mathbf{w}} \in \arg \min_{\mathbf{w} \in \Delta^{J-1}} \frac{1}{T_0} \sum_{t=1}^{T_0} d^2(Y_{1,t}, Y_{2:J+1,t}^{(\mathbf{w})}),$$

where the synthetic control at time t is defined through the weighted Fréchet mean

$$Y_{2:J+1,t}^{(\mathbf{w})} = \arg \min_{\nu \in \mathcal{M}} \sum_{j=2}^{J+1} w_j d^2(\nu, Y_{j,t}).$$

For the GSDID estimator, both unit and time weights are estimated. The unit weights w are obtained in the same way as for GSC, while the time weights $\bar{\boldsymbol{\lambda}} \in \Delta^{T_0-1}$ are determined by matching the pre-treatment and post-treatment trajectories of the control units,

$$\bar{\boldsymbol{\lambda}} \in \arg \min_{\boldsymbol{\lambda} \in \Delta^{T_0-1}} \frac{1}{J} \sum_{j=2}^{J+1} d^2(Y_{j,T_0+1:T}^{(\oplus)}, Y_{j,1:T_0}^{(\boldsymbol{\lambda})}),$$

where $Y_{j,T_0+1:T}^{(\oplus)}$ denotes the post-treatment Fréchet mean of unit j and $Y_{j,1:T_0}^{(\boldsymbol{\lambda})}$ the weighted pre-treatment Fréchet mean.

In both cases, the optimization is carried out over the probability simplex, with the geometry of the underlying metric space determining how the Fréchet means are evaluated.

S.3.3 Spaces with closed-form weighted Fréchet means

For networks (Example 1), symmetric positive-definite matrices (Example 3), distributions (Example 4), and functional data (Example 5), the weighted Fréchet mean admits an explicit expression under the metrics considered in this paper. In these cases, the outer

optimization problems in Section S.3.2 reduce to convex quadratic programs in w (and λ), which can be solved efficiently using standard quadratic programming solvers such as OSQP (Stellato et al., 2020). This yields numerically stable and fast implementations.

S.3.4 Compositional data

For compositional data (Example 2), the situation is more complex. When mapped to the positive orthant of the sphere, the weighted Fréchet mean has no closed form and must be obtained via iterative algorithms on the manifold. Each evaluation of the objective therefore requires solving an inner Fréchet mean problem, which creates a bilevel optimization problem. Because analytical differentiation is intractable in this nonlinear setting, we employ a derivative-free constrained optimization strategy, specifically the COBYLA algorithm (Powell, 1994) as implemented in the `nloptr` package (Johnson, 2008). The inner Fréchet mean computations are carried out using the `manifold` package (Dai et al., 2021).

S.3.5 Practical remarks

For the tractable cases with closed-form weighted Fréchet means, optimization is straightforward and stable. For compositional data, convergence of the iterative mean calculation can be slow when many observations lie close to zero components, in which case regularization (e.g., adding a small constant to proportions before normalization) improves stability.

S.4 Verification of Assumption 3.1

To verify that the causal models for Examples 1–5 given in Section 2 satisfy Assumption 3.1, recall that $\bar{\mathbf{w}} \in \arg \min_{\mathbf{w} \in \Delta^{J-1}} \frac{1}{T_0} \sum_{t=1}^{T_0} d^2(Y_{1,t}, Y_{2:J+1,t}^{(\mathbf{w})})$. For $\mathbf{w} = (w_2, \dots, w_{J+1})' \in \Delta^{J-1}$, define

$$U_{2:J+1}^{(\mathbf{w})} = \arg \min_{\nu \in \mathcal{M}} \sum_{j=2}^{J+1} w_j d^2(\nu, U_j),$$

and $\mathbb{W}^* = \{\mathbf{w} \in \Delta^{J-1} : d(U_1, U_{2:J+1}^{(\mathbf{w})}) = 0\}$. Throughout Sections S.4.1–S.4.5 below, we assume that \mathbb{W}^* is not empty.

S.4.1 Space of networks with the Frobenius metric

Recall that $Y_{j,t}(N)$ is given as

$$\begin{aligned} Y_{j,t}(N) &= g_t(U_j) := \gamma_{\mu_t, U_j}(\alpha_t) \\ &= \mu_t + \alpha_t(U_j - \mu_t), \quad \alpha_t \in (0, 1). \end{aligned}$$

For $\mathbf{w} \in \Delta^{J-1}$,

$$\begin{aligned} U_{2:J+1}^{(\mathbf{w})} &= \sum_{j=2}^{J+1} w_j U_j, \\ g_t^{(\mathbf{w})}(U_{2:J+1}) &= \sum_{j=2}^{J+1} w_j Y_{j,t}(N) = \sum_{j=2}^{J+1} w_j \{\mu_t + \alpha_t(U_j - \mu_t)\} \\ &= \mu_t + \alpha_t \left\{ \sum_{j=2}^{J+1} w_j U_j - \mu_t \right\} = \mu_t + \alpha_t(U_{2:J+1}^{(\mathbf{w})} - \mu_t) = g_t(U_{2:J+1}^{(\mathbf{w})}). \end{aligned} \quad (\text{S5})$$

Furthermore,

$$\begin{aligned} d_F^2(Y_{1,t}(N), Y_{2:J+1,t}^{(\mathbf{w})}) &= d_F^2(g_t(U_1), g_t(U_{2:J+1}^{(\mathbf{w})})) \\ &= \text{tr} \left\{ (g_t(U_1) - g_t(U_{2:J+1}^{(\mathbf{w})}))' (g_t(U_1) - g_t(U_{2:J+1}^{(\mathbf{w})})) \right\} \\ &= \alpha_t^2 \text{tr} \left\{ (U_1 - U_{2:J+1}^{(\mathbf{w})})' (U_1 - U_{2:J+1}^{(\mathbf{w})}) \right\} \\ &= \alpha_t^2 d_F^2(U_1, U_{2:J+1}^{(\mathbf{w})}), \end{aligned} \quad (\text{S6})$$

where $\text{tr}(A)$ is the trace of the matrix A . This yields $\bigcap_{t=1}^{T_0} \mathbb{W}_t^* = \bigcap_{t=T_0+1}^T \mathbb{W}_t^* = \mathbb{W}^*$ and hence Assumption 3.1 holds.

S.4.2 Space of compositional data with the arc-length distance

Recall that $Y_{j,t}(N)$ is defined as

$$Y_{j,t}(N) = g_t(U_j) = \text{Exp}_{\mu_t}(A_t \text{Log}_{U_1}(U_j)), \quad \mu_t \in \mathcal{M}.$$

Note that $Y_{1,t} = \text{Exp}_{\mu_t}(0) = \mu_t$. Define $F_{\mathbf{w}}(\nu) = \sum_{j=2}^{J+1} w_j d^2(\nu, g_t(U_j))$, $\mathbf{w} \in \Delta^{J-1}$ and let $\text{grad}(F_{\mathbf{w}}(\nu))$ denote the gradient at $\nu \in \mathcal{M}$. Throughout we assume here that among the elements $g_t(U_2), \dots, g_t(U_{J+1})$, at least one is in the interior of \mathcal{S}_+^{d-1} . Then Theorem 1 in [Buss and Fillmore \(2001\)](#) implies that Assumption 3.1(i) holds. For a more general discussion on sufficient conditions for the uniqueness of the Fréchet mean of a distribution on a Riemannian manifold, see Remark 2.8 in [Eltzner and Huckemann \(2019\)](#) and the references therein. For $\overline{\mathbb{W}}_t^* = \{\mathbf{w} \in \Delta^{J-1} : \sum_{j=2}^{J+1} w_j \text{Log}_{g_t(U_1)}(g_t(U_j)) = 0\}$ one can show that Assumption 3.1(ii) holds if

$$\mathbb{W}_t^* = \overline{\mathbb{W}}_t^*. \quad (\text{S7})$$

Indeed, we have

$$\begin{aligned} \mathbb{W}_t^* &= \overline{\mathbb{W}}_t^* = \{\mathbf{w} \in \Delta^{J-1} : \sum_{j=2}^{J+1} w_j \text{Log}_{\mu_t} \{\text{Exp}_{\mu_t}(A_t \text{Log}_{U_1}(U_j))\} = 0\} \\ &= \{\mathbf{w} \in \Delta^{J-1} : A_t \sum_{j=2}^{J+1} w_j \text{Log}_{U_1}(U_j) = 0\} \\ &= \{\mathbf{w} \in \Delta^{J-1} : \sum_{j=2}^{J+1} w_j \text{Log}_{U_1}(U_j) = 0\} = \mathbb{W}^*. \end{aligned}$$

This yields $\bigcap_{t=1}^{T_0} \mathbb{W}_t^* = \bigcap_{t=T_0+1}^T \mathbb{W}_t^* = \mathbb{W}^*$ and hence Assumption 3.1(ii) holds.

Next we show (S7). Specifically, we establish (i) $\mathbb{W}_t^* \subset \overline{\mathbb{W}}_t^*$ and (ii) $\mathbb{W}_t^* \supset \overline{\mathbb{W}}_t^*$.

Proof of (i): Fix an arbitrary $\mathbf{w} = (w_2, \dots, w_{J+1})' \in \mathbb{W}_t^*$. By definition, $g_t^{(\mathbf{w})}(U_{2:J+1})$ is a Fréchet mean of the distribution of a random element X such that $\Pr(X = g_t(U_j)) = w_j$, $j = 2, \dots, J+1$. Further, the condition $d(g_t(U_1), g_t^{(\mathbf{w})}(U_{2:J+1})) = 0$ yields $g_t(U_1) = g_t^{(\mathbf{w})}(U_{2:J+1})$. Applying Corollary 3 in [Le and Barden \(2014\)](#), we then have $\sum_{j=2}^{J+1} w_j \text{Log}_{g_t(U_1)}(g_t(U_j)) = 0$. This implies $\mathbf{w} \in \overline{\mathbb{W}}_t^*$ and hence $\mathbb{W}_t^* \subset \overline{\mathbb{W}}_t^*$ holds.

Proof of (ii): Fix an arbitrary $\mathbf{w} = (w_2, \dots, w_{J+1})' \in \overline{\mathbb{W}}_t^*$. From the definition of $\overline{\mathbb{W}}_t^*$ and the uniqueness of the Fréchet mean, Theorem 1 in [Buss and Fillmore \(2001\)](#) yields $g_t(U_1) = g_t^{(\mathbf{w})}(U_{2:J+1})$. This implies $\mathbf{w} \in \mathbb{W}_t^*$ and hence $\mathbb{W}_t^* \supset \overline{\mathbb{W}}_t^*$.

S.4.3 Space of SPD matrices

First, we consider the space of SPD matrices with the Frobenius metric. Standard arguments lead to (S5) and (S6). Hence Assumption 3.1 holds.

Second, we consider the space of SPD matrices with the power metric family defined as

$$d_{F,p}(A, B) = \|F_p(A) - F_p(B)\|_F,$$

where $p > 0$ is a constant, $\|\cdot\|_F$ is the Frobenius metric, and F_p is a matrix power map defined as

$$F_p(A) = A^p = U\Lambda^p U' : \text{Sym}_m^+ \rightarrow \text{Sym}_m^+,$$

where $U\Lambda U'$ is the usual spectral decomposition of $A \in \text{Sym}_m^+$. The geodesic with respect to $d_{F,p}$ between A and B is given as

$$\gamma_{A,B}(t) = [A^p + t(B^p - A^p)]^{1/p} = F_{1/p}(A^p + t(B^p - A^p)).$$

Recall that $Y_{j,t}(N)$ is given as $Y_{j,t}(N) = g_t(U_j) = \gamma_{\mu_t, U_j}(\alpha_t)$. For $\mathbf{w} \in \Delta^{J-1}$,

$$\begin{aligned} (U_{2:J+1}^{(\mathbf{w})})^p &= \sum_{j=2}^{J+1} w_j U_j^p, \\ (g_t^{(\mathbf{w})}(U_{2:J+1}))^p &= \mu_t^p + \alpha_t \left\{ \sum_{j=2}^{J+1} w_j U_j^p - \mu_t^p \right\} = (g_t(U_{2:J+1}^{(\mathbf{w})}))^p. \end{aligned}$$

Furthermore,

$$\begin{aligned} d_{F,p}^2(Y_{1,t}(N), Y_{2:J+1,t}^{(\mathbf{w})}) &= \|(Y_{1,t}(N))^p - (Y_{2:J+1,t}^{(\mathbf{w})})^p\|_F^2 = \|(g_t(U_1))^p - (g_t(U_{2:J+1}^{(\mathbf{w})}))^p\|_F^2 \\ &= \alpha_t^2 \|U_1^p - \sum_{j=2}^{J+1} w_j U_j^p\|_F^2 = \alpha_t^2 d_{F,p}^2(U_1, U_{2:J+1}^{(\mathbf{w})}). \end{aligned}$$

This yields $\bigcap_{t=1}^{T_0} \mathbb{W}_t^* = \bigcap_{t=T_0+1}^T \mathbb{W}_t^* = \mathbb{W}^*$ and hence Assumption 3.1 holds.

Third, we consider the space of SPD matrices with the Log-Euclidean metric,

$$d_{\text{LE}}(A, B) = \|\log(A) - \log(B)\|_F.$$

The geodesic with respect to d_{LE} between A and B is

$$\gamma_{A,B}(t) = \exp(\log A + t(\log B - \log A)).$$

Recall $Y_{j,t}(N) = g_t(U_j) = \gamma_{\mu_t, U_j}(\alpha_t)$. For $\mathbf{w} \in \Delta^{J-1}$,

$$\begin{aligned} \log(U_{2:J+1}^{(\mathbf{w})}) &= \sum_{j=2}^{J+1} w_j \log(U_j), \\ \log(g_t^{(\mathbf{w})}(U_{2:J+1})) &= \log(\mu_t) + \alpha_t \left(\sum_{j=2}^{J+1} w_j \log(U_j) - \log(\mu_t) \right) = \log(g_t(U_{2:J+1}^{(\mathbf{w})})). \end{aligned}$$

Further,

$$\begin{aligned} d_{\text{LE}}^2(Y_{1,t}(N), Y_{2:J+1,t}^{(\mathbf{w})}) &= \|\log(Y_{1,t}(N)) - \log(Y_{2:J+1,t}^{(\mathbf{w})})\|_F^2 = \|\log(g_t(U_1)) - \log(g_t(U_{2:J+1}^{(\mathbf{w})}))\|_F^2 \\ &= \alpha_t^2 \|\log(U_1) - \sum_{j=2}^{J+1} w_j \log(U_j)\|_F^2 = \alpha_t^2 d_{\text{LE}}^2(U_1, U_{2:J+1}^{(\mathbf{w})}). \end{aligned}$$

This yields $\bigcap_{t=1}^{T_0} \mathbb{W}_t^* = \bigcap_{t=T_0+1}^T \mathbb{W}_t^* = \mathbb{W}^*$ and hence Assumption 3.1 holds.

Fourth, we consider the space of SPD matrices with the Log-Cholesky metric. The Log-Cholesky metric is defined as

$$d_{\text{LC}}(L_1, L_2) = \left\{ \|\lfloor L_1 \rfloor - \lfloor L_2 \rfloor\|_F^2 + \|\log(\mathbb{D}(L_1)) - \log(\mathbb{D}(L_2))\|_F^2 \right\}^{1/2}.$$

Note that the space $(\mathcal{L}_m^+, d_{\text{LC}})$ is a geodesic metric space (Lin, 2019) and the geodesic with respect to d_{LC} between L_1 and L_2 is

$$\gamma_{L_1, L_2}(t) = \lfloor L_1 \rfloor + t(\lfloor L_2 \rfloor - \lfloor L_1 \rfloor) + \exp \{ \log(\mathbb{D}(L_1)) + t(\log(\mathbb{D}(L_2)) - \log(\mathbb{D}(L_1))) \}.$$

Let $U_j \in \mathcal{L}_m^+$, $j = 1, \dots, J+1$ and $\mu_t \in \mathcal{L}_m^+$, $t = 1, \dots, T$. Recall that $Y_{j,t}(N) = g_t(U_j) = \gamma_{\mu_t, U_j}(\alpha_t)$. For $\mathbf{w} \in \Delta^{J-1}$,

$$\lfloor (U_{2:J+1}^{(\mathbf{w})}) \rfloor = \sum_{j=2}^{J+1} w_j \lfloor U_j \rfloor, \quad \log(\mathbb{D}(U_{2:J+1}^{(\mathbf{w})})) = \sum_{j=2}^{J+1} w_j \log(\mathbb{D}(U_j)).$$

Further,

$$\begin{aligned} \lfloor g_t^{(\mathbf{w})}(U_{2:J+1}) \rfloor &= \lfloor \mu_t \rfloor + \alpha_t \left\{ \sum_{j=2}^{J+1} w_j \lfloor U_j \rfloor - \lfloor \mu_t \rfloor \right\} = \lfloor g_t(U_{2:J+1}^{(\mathbf{w})}) \rfloor, \\ \log(\mathbb{D}(g_t^{(\mathbf{w})}(U_{2:J+1}))) &= \log(\mathbb{D}(\mu_t)) + \alpha_t \left\{ \sum_{j=2}^{J+1} w_j \log(\mathbb{D}(U_j)) - \log(\mathbb{D}(\mu_t)) \right\} \\ &= \log(\mathbb{D}(g_t(U_{2:J+1}^{(\mathbf{w})}))). \end{aligned}$$

Then

$$\begin{aligned}
& d_{\text{LC}}^2(Y_{1,t}(N), Y_{2:J+1,t}^{(\mathbf{w})}) \\
&= \| \lfloor g_t(U_1) \rfloor - \lfloor g_t(U_{2:J+1}^{(\mathbf{w})}) \rfloor \|_F^2 + \| \log(\mathbb{D}(g_t(U_1))) - \log(\mathbb{D}(g_t(U_{2:J+1}^{(\mathbf{w})}))) \|_F^2 \\
&= \alpha_t^2 \| \lfloor U_1 \rfloor - \sum_{j=2}^{J+1} w_j \lfloor U_j \rfloor \|_F^2 + \alpha_t^2 \| \log(\mathbb{D}(U_1)) - \sum_{j=2}^{J+1} w_j \log(\mathbb{D}(U_j)) \|_F^2 \\
&= \alpha_t^2 d_{\text{LC}}^2(U_1, U_{2:J+1}^{(\mathbf{w})}).
\end{aligned}$$

This yields $\bigcap_{t=1}^{T_0} \mathbb{W}_t^* = \bigcap_{t=T_0+1}^T \mathbb{W}_t^* = \mathbb{W}^*$ and hence Assumption 3.1 holds.

S.4.4 Space of univariate probability distributions with the 2-Wasserstein distance

Recall that $Y_{j,t}(N) = g_t(U_j) := \gamma_{\mu_t, U_j}(\alpha_t)$, $\alpha_t \in (0, 1)$. Then we have $F_{Y_{j,t}(N)}^{-1}(\cdot) = F_{\mu_t}^{-1}(\cdot) + \alpha_t(F_{U_j}^{-1}(\cdot) - F_{\mu_t}^{-1}(\cdot))$.

For $\mathbf{w} \in \Delta^{J-1}$,

$$\begin{aligned}
F_{U_{2:J+1}^{(\mathbf{w})}}^{-1}(\cdot) &= \sum_{j=2}^{J+1} w_j F_{U_j}^{-1}(\cdot), \\
F_{g_t^{(\mathbf{w})}(U_{2:J+1})}^{-1}(\cdot) &= \sum_{j=2}^{J+1} w_j F_{Y_{j,t}(N)}^{-1}(\cdot) = \sum_{j=2}^{J+1} w_j \left\{ F_{\mu_t}^{-1}(\cdot) + \alpha_t(F_{U_j}^{-1}(\cdot) - F_{\mu_t}^{-1}(\cdot)) \right\} \\
&= F_{\mu_t}^{-1}(\cdot) + \alpha_t \left\{ \sum_{j=2}^{J+1} w_j F_{U_j}^{-1}(\cdot) - F_{\mu_t}^{-1}(\cdot) \right\} = \left(F_{\gamma_{\mu_t, U_{2:J+1}^{(\mathbf{w})}}(\alpha_t)}^{-1} \right)^{-1}(\cdot) \\
&= F_{g_t(U_{2:J+1}^{(\mathbf{w})})}^{-1}(\cdot).
\end{aligned}$$

Furthermore,

$$\begin{aligned}
d_{\mathcal{W}}^2(Y_{1,t}(N), Y_{2:J+1,t}^{(\mathbf{w})}) &= d_{\mathcal{W}}^2(g_t(U_1), g_t(U_{2:J+1}^{(\mathbf{w})})) = \alpha_t^2 \int_0^1 \left\{ F_{U_1}^{-1}(p) - \sum_{j=2}^{J+1} w_j F_{U_j}^{-1}(p) \right\}^2 dp \\
&= \alpha_t^2 d_{\mathcal{W}}^2(U_1, U_{2:J+1}^{(\mathbf{w})}),
\end{aligned}$$

which yields $\bigcap_{t=1}^{T_0} \mathbb{W}_t^* = \bigcap_{t=T_0+1}^T \mathbb{W}_t^* = \mathbb{W}^*$ and hence Assumption 3.1 holds.

S.4.5 Space of functional data with the L^2 metric

Note that

$$(Y_{j,t}(N))(s) = (\gamma_{\mu_t, U_j}(\alpha_t))(s) = \mu_t(s) + \alpha_t(U_j(s) - \mu_t(s)), \quad s \in \mathcal{T}.$$

For $\mathbf{w} \in \Delta^{J-1}$,

$$\begin{aligned} U_{2:J+1}^{(\mathbf{w})}(s) &= \sum_{j=2}^{J+1} w_j U_j(s), \\ (g_t^{(\mathbf{w})}(U_{2:J+1}))(s) &= \sum_{j=2}^{J+1} w_j (Y_{j,t}(N))(s) \\ &= \mu_t(s) + \alpha_t(U_{2:J+1}^{(\mathbf{w})}(s) - \mu_t(s)) = (g_t(U_{2:J+1}^{(\mathbf{w})}))(s), \quad s \in \mathcal{T}. \end{aligned}$$

Next,

$$\begin{aligned} d_{L^2}^2(Y_{1,t}(N), Y_{2:J+1,t}^{(\mathbf{w})}) &= d_{L^2}(g_t(U_1), g_t(U_{2:J+1}^{(\mathbf{w})})) = \int_{\mathcal{T}} \left\{ (g_t(U_1))(s) - (g_t(U_{2:J+1}^{(\mathbf{w})}))(s) \right\}^2 ds \\ &= \alpha_t^2 \int_{\mathcal{T}} \left\{ U_1(s) - U_{2:J+1}^{(\mathbf{w})}(s) \right\}^2 ds = \alpha_t^2 d_{L^2}(U_1, U_{2:J+1}^{(\mathbf{w})}), \end{aligned}$$

which gives $\bigcap_{t=1}^{T_0} \mathbb{W}_t^* = \bigcap_{t=T_0+1}^T \mathbb{W}_t^* = \mathbb{W}^*$ and hence Assumption 3.1 holds.

S.5 Proofs

S.5.1 Proof of Theorem 3.1

Observe that

$$\bar{\mathbf{w}} \in \arg \min_{\mathbf{w} \in \Delta^{J-1}} \frac{1}{T_0} \sum_{t=1}^{T_0} d^2(g_t(U_1), g_t^{(\mathbf{w})}(U_{2:J+1})).$$

Then Assumption 3.1(ii) yields $\bar{\mathbf{w}} \in \bigcap_{t=T_0+1}^T \mathbb{W}_t^*$ and hence

$$Y_{1,t}^{(\text{GSC})} = g_t^{(\bar{\mathbf{w}})}(U_{2:J+1}) = g_t(U_1) = Y_{1,t}(N), \quad t = T_0 + 1, \dots, T.$$

S.5.2 Proof of Proposition S1

From the definition of the binary relation \sim on $\mathcal{G}(\mathcal{M})$, we have

$$Y_{1,t}(N) = \Gamma_{Y_{1,t}^{(\text{GSC})}, Y_{1,t}(N)}(Y_{1,t}^{(\text{GSC})}) = \Gamma_{m_t^{(\bar{w})}(\mathbf{Z}_{2:J+1,1:T_0}), m_t(\mathbf{Z}_{1,1:T_0})}(Y_{1,t}^{(\text{GSC})}).$$

S.5.3 Proof of Theorem S1

Note that under Assumption S2, we have

$$\begin{aligned} Y_{2:J+1,1:T_0}^{(\bar{w}, \bar{\lambda})} &= g^{(\bar{w}, \bar{\lambda})}(U_{2:J+1}, V_{1:T_0}), \quad Y_{2:J+1,T_0+1:T}^{(\bar{w}, \oplus)} = g^{(\bar{w}, \oplus)}(U_{2:J+1}, V_{T_0+1:T}), \\ Y_{1,1:T_0}^{(\bar{\lambda})} &= g^{(\bar{\lambda})}(U_1, V_{1:T_0}). \end{aligned}$$

To show (S4) under Assumption S3, observe that

$$\bar{w} \in \arg \min_{w \in \Delta^{J-1}} \frac{1}{T_0} \sum_{t=1}^{T_0} d^2(g(U_1, V_t), g^{(w)}(U_{2:J+1}, V_t)).$$

This yields $\bar{w} \in \mathbb{W}_{\lambda}^* \cap \mathbb{W}_{\oplus}^*$ and hence

$$Y_{2:J+1,1:T_0}^{(\bar{w}, \bar{\lambda})} = g^{(\bar{\lambda})}(U_1, V_{1:T_0}), \quad Y_{2:J+1,T_0+1:T}^{(\bar{w}, \oplus)} = g^{(\oplus)}(U_1, V_{T_0+1:T}).$$

Then we have

$$\begin{aligned} Y_{1,T_0+1:T}^{(\text{GSDID})} &= \Gamma_{g^{(\bar{\lambda})}(U_1, V_{1:T_0}), g^{(\oplus)}(U_1, V_{T_0+1:T})} \left(g^{(\bar{\lambda})}(U_1, V_{1:T_0}) \right) \\ &= g^{(\oplus)}(U_1, V_{T_0+1:T}) = Y_{1,T_0+1:T}^{(\oplus)}(N). \end{aligned}$$

To show (S4) under Assumption S4, observe that

$$\bar{\lambda} \in \arg \min_{\lambda \in \Delta^{T_0-1}} \sum_{j=2}^{J+1} d^2(g^{(\oplus)}(U_j, V_{T_0+1:T}), g^{(\lambda)}(U_j, V_{1:T_0})).$$

Then Assumption S4 yields $\bar{\lambda} \in \bigcap_{j=1}^{J+1} \Lambda_j^*$ and hence

$$\begin{aligned} Y_{1,T_0+1:T}^{(\text{GSDID})} &= \Gamma_{g^{(\bar{w}, \bar{\lambda})}(U_{2:J+1}, V_{1:T_0}), g^{(\bar{w}, \oplus)}(U_{2:J+1}, V_{T_0+1:T})} \left(g^{(\bar{\lambda})}(U_1, V_{1:T_0}) \right) \\ &= g^{(\oplus)}(U_1, V_{T_0+1:T}) = Y_{1,T_0+1:T}^{(\oplus)}(N). \end{aligned}$$

This completes the proof.